Wilfrid Laurier University

Scholars Commons @ Laurier

Theses and Dissertations (Comprehensive)

2019

High resolution spatial variability in spring snowmelt for an Arctic shrub-tundra watershed

Branden J. Walker
Wilfrid Laurier University, bwalker@wlu.ca

Philip Marsh Dr
Wilfrid Laurier University, pmarsh@wlu.ca

Follow this and additional works at: https://scholars.wlu.ca/etd

Part of the Hydrology Commons

High resolution spatial variability in spring snowmelt for an Arctic shrub-tundra watershed

by

Branden J. Walker

(B.A. Geography, Wilfrid Laurier University, 2015)

THESIS

Submitted to the Department of Geography and Environmental Studies

in fulfilment of the requirements for

Master of Science in Geography

Wilfrid Laurier University
© Branden Walker 2018

Table of Contents

Index of Figures

Index of Tables

Index of Appendix

Acknowledgements

To my wife, Hannah. Thank You for all your support over the past few years. I cannot express my gratitude in words for how loving and supportive you have been. I would like to say Thank You for always being there no matter the geographical separation between us.

To my supervisor, Dr. Marsh, I would like to express my gratitude for this opportunity to explore Canada's North and be a part of the Trail Valley Creek research group. It has been a pleasure to work alongside - and with you- for the past few years as part of the Trail Valley Creek research station. I had never thought I would get to visit the Northwest Territories. Thank You for your support and guidance over these past few years.

To the numerous people who assisted in the field work (either directly or indirectly). I would especially like to thank Philip Mann, Tyler DeJong, Alex MacLean, Gabriel Hould Gosselin and Evan Wilcox for all their assistance in the field over the past few years. You have all contributed in one way or another to this thesis and your hard work is greatly appreciated. Also, to the many others thanks for making the time spent in camp and the office enjoyable and productive. To those whose names I did not mention I apologize- but Thank You for the hard field days and fun times in the field.

Chapter 1 : Introduction and background

Seasonal snow plays a significant role in Arctic ecosystems, where snow typically covers the ground seven to nine months of the year. In these environments, the snowpack distribution and melt timing act as important regulators for available water in the ecosystem and control many environmental variables such as soil temperatures, active layer depths, vegetation and permafrost (Kokelj and Burn, 2005; Lantz et al., 2013, 2010; O'Neill and Burn, 2016). In Arctic environments the release of accumulated precipitation in the form of snowmelt is the most hydrologically important event and often releasing over 75 percent of the annual discharge (Bring et al., 2016; Marsh et al., 1995; Marsh and Woo, 1981; Mielko and Woo, 2006).

Warming air temperatures linked to anthropogenic climate change is significantly amplified relative to southern regions (IPCC, 2013), and has resulted in environmental change across the Arctic (IPCC, 2013). Increased (though decreased in a few regions) snow precipitation, increased rain-on-snow events, and earlier snowmelt dates are some of the numerous changes expected to be observed across Arctic-tundra environments. Cumulatively, these will result in drastic changes to the hydrological regimes, specifically with relation to the snow hydrology and spring snowmelt.

Currently, there is uncertainty in how a warming climate will affect spring stream discharge (commonly referred to as spring freshet) of these northern nival basins. Recent observational and modelling studies synthesized by the IPCC (2013) suggest that warmer spring air temperatures and earlier spring snowmelt initiations would simply result in increased snowmelt rates and an earlier spring freshet. Pohl and Marsh, (2006) for example suggested this type of change for the western Canadian Arctic. However, the effects of a warming climate on the spring snowcover and freshet discharge may not

be as well understood as once thought. Musselman *et al.*, (2017) recently showed demonstrated that for western North America the onset of an earlier snowmelt is accompanied by decreased snowmelt rates. Shi *et al.* (2015) found no change, and in some cases delayed timing of spring snowmelt freshet for an Arctic-tundra stream, even though there was a strong trend towards earlier snowmelt initiation date over the 27 year study period. The reason for such unexpected changes is poorly understood, but may be related to complex relationships between snow, shrubs and active layer for example. Current hydrological or land surface models are unable to simulate such hydrological changes in response to a warming climate. Recent studies (Sivapalan, 2018) are suggesting that micro-scale snowmelt processes, typically ignored in current generation models, dominate streamflow response, and as a result there is an urgent need to improve or understand of key snowmelt runoff processes.

The research in this thesis attempts to provide a better understanding of these complex hydrological systems by studying micro-scale (ranging from square meter to hillslope scale) snowmelt conditions using high-resolution remote sensing datasets. The objectives of this study are to:

1) provide insight into the micro-scale variability of the snow cover and snowmelt patterns of an Arctic-tundra catchment over the duration of the spring snowmelt, and

2) quantify the spatial and temporal variability in snow conditions and snowpack ablation across various land cover types.

The results of this study will provide a comprehensive high-resolution dataset of snow cover characteristics across the spring snowmelt period that can be coupled with traditional hydrological methods such as snow surveys, eddy covariance, and

streamflow measurements to create datasets suited towards integration with future high-resolution spatially distributed hydrological models.

This thesis follows a manuscript-style outline, with the first chapter presenting an in-depth literature review of Arctic-tundra snow, snowmelt processes, and traditional methods of measuring snow cover, followed by an overview of the research objectives and study site. Chapter 2 uses in-situ observations of snowpack density and *Structure-from-Motion* snow depths created using Unmanned Aerial Systems (UAS) to measure micro-scale changes in snow cover for a tundra catchment over the spring melt period. This chapter provides and in-depth analysis of the 2015-16 spring snowmelt with a focus on micro-scale variability in snowpack conditions across the snowmelt, providing direct measurements of the impacts of vegetation and topographic drifts on snowmelt patterns. Chapter 3 summarizes the thesis and includes a brief discussion on the application of UAS for snow hydrology.

Literature Review

Arctic-tundra snow

Snow cover plays a vital role across Arctic tundra landscapes affecting the local, regional, and even global-scale water and energy balances (Pomeroy, 2005), permafrost (Marsh et al., 2010) and vegetation (Lantz et al., 2013; Liston et al., 2002; Sturm et al., 2001). Snow is hydrologically the most important variable for northern environments with snowcover persisting for seven to nine months and accounts for over half of the annual precipitation. Kane et al. (1991) noted that end-of-winter snow cover accounted for nearly 40 percent of the annual precipitation in southern Arctic regions, but may account for as much as 80 percent in more northern regions of the Arctic

(Prowse and Ommanney, 1990; Young et al., 2006). Snow, measured as snow water equivalent (SWE) is clearly important for Arctic hydrology, however our ability to accurately measure and model SWE for tundra regions has proven difficult as snowcover is not uniformly distributed within the basin.

During the winter months wind transportation and deposition is the dominant transportation method for the movement of water across the landscape (Pomeroy and Schmidt, 1993). The process of redistribution in tundra environments results in localized deposits of high SWE in the form of drifts in the lower stream channels, vegetation patches and on the lee of hillslopes (Marsh et al., 2008). Snow drifts play a significant role in Arctic-tundra environments because they contain substantial quantities of water released as meltwater runoff at a slower rate relative to the surrounding tundra landscape. Deeper snow drifts are also important from a hydrological perspective because they often remain weeks after the tundra hilltops have melted away, providing the streams with melt water, and resulting in relatively high flow rate long after the initial melt (Marsh and Woo, 1981; Quinton et al., 2004; Quinton and Marsh, 1998a).

Our ability to quantify snow in these environments is further challenged by the current inability to accurately measure snowfall during the winter months. Direct measurement of snowfall can be difficult due to very large errors in gauge under catch, primarily from the effects of wind speed, with snowfall typically underestimated by 10 to 120% across the Arctic (Goodison et al., 1998; Pan et al., 2016; Yang et al., 2005). Ongoing research is attempting to solve this problem, but with limited success to date (Macdonald and Pomeroy, 2007; Mann, 2018; Thériault et al., 2012). Accurate measurements of snowfall are further challenged by declines in snow over the winter

from sublimation. In Arctic tundra environments blowing snow results in an estimated sublimation rate of 20% to 40% of winter snowfall (Pomeroy et al., 1999, 1997; Pomeroy and Gray, 1995), but this estimate likely has extremely high errors as extreme winter conditions make sublimation rates variable, and gathering measurements extremely challenging and dangerous. Blowing snow events lead to spatially distributed end-of-winter snowpacks with drift features that cover a small area but contain a large portion of the snow water equivalent. Accurately measuring the distributed snowpack in Arctic tundra environments has proven difficult using traditional observation methods (Pohl and Marsh, 2006; Rees et al., 2014), modelling (Pomeroy et al., 1997), and remote sensing techniques (Dietz et al., 2012), where estimates of basin snow are complicated by issues of scale, sampling bias, and an inability to accurately measure small-scale localized snow deposits. Further complications arise when measuring changes to basin snowcover over the spring melt as accessibility is greatly reduced as transportation over the snow is limited.

Snowmelt begins when absorbed solar radiation begins to increase which typically coincides with air surface temperatures rising above 0°C for a given amount of time. With the onset of snowmelt, occurring as snow reaches an isothermal 0°C, wet snow metamorphism processes transform the snowpack resulting in an increase in mean snow grain size, disappearance of smaller snow grains over time, and a general rounding of the grains (Colbeck, 1982, 1979; Marsh, 1987). The introduction of liquid water into a snowpack results in a growth of larger snow grains at the expense of smaller grains, and allowing for the release of latent heat as liquid water refreezes in dryer portions of the snowpack (Colbeck, 1982). The introduction of liquid water

therefore results in an overall increase in snowpack density with a transition from the pendular (low liquid water content) to the funicular (high water content) regimes (Colbeck, 1979).

The stage known as the *warming phase* occurs as the snowpack is warmed to an isothermal 0°C, after which vertical movement of meltwater within the snowpack is initiated. The amount of energy required to raise the snowpack to an isothermal 0°C is known as the *cold content*. Once isothermal, additional input of energy leads to the formation of liquid water that collects in the pore space of the snowpack. Once all the available pore space is filled with liquid water the snowpack is said to be "ripe"- correspondingly this stage in snow pack metamorphism is termed the *ripening phase*. Theoretically, lateral runoff at the base of the snowpack can only occur when the snowpack has completed both the warming and ripening phases of snowmelt, however studies have shown that meltwater runoff can be expediated through intra-snowpack flow fingers (Marsh and Woo, 1984; Waldner et al., 2004).

Snowmelt occurs heterogeneously across Arctic environments due to the unevenly distributed nature of the snowpack at the end of winter. Accordingly, snowmelt completion dates vary significantly across the landscape and can have large local and regional impacts on snowmelt runoff and the spring freshet. A large contributing factor to snowmelt timing is the aspect (orientation of the slope) of the snowpack. In tundra environments, south-facing slopes receive more incoming solar radiation and therefore often melt at an earlier date (Marsh et al., 2010). Furthermore, snowpacks within highly vegetated areas, such as forest stands or large shrub patches, tend to receive less incoming solar radiation due to the low sun inclination during the spring period and

shading from the vegetation (Marsh et al., 2010), however the effects of vegetation canopy has also been observed to expediate the snowmelt rates (Marsh et al., 2010; Pomeroy et al., 2006; Whittington et al., 2012).

Interactions between shrub vegetation and end-of-winter snowpack distribution have been documented across shrub-tundra environments (Rees et al., 2014; Sturm et al., 2005), but the affects of vegetation on snow hydrology do not only influence the snowpack distribution during the winter months. Interactions between shrub cover and snow continue into the spring melt period where vegetation cover holds an integral role controlling basin-scale snowmelt patterns. In a study of spatio-temporal melt patterns for and Arctic shrub-tundra basin, Pohl and Marsh, (2006) found similar snowpack depletion timing for open-tundra and shrub-tundra patches, despite the later containing 40% more end-of-winter SWE. Similar melt completion dates were concluded to be a result of increased melt rates in tall shrub patches caused by exposed canopy above the snowpack. During the winter months many tall shrubs become buried within the snowpack. With the onset of melt, shrubs often rebound above the snow reducing the surface albedo and increased outgoing longwave radiation and sensible heat flux causing localized melt around the shrub stems (Pohl and Marsh, 2006). However, emergence of the shrub canopy during the melt did reduce incoming solar radiation through shading and lowered the wind speed above the snowpack. In a similar study, Pomeroy *et al.* (2006) documented similar phenomenon for both short and tall shrub canopies concluding shrub canopy resulted in increased longwave radiation and sensible heat flux emitted from the shrubs to the atmosphere and snowpack effectively expediating the melt rates in these area. In their study on alpine shrub tundra, Pomeroy

et al. (2006) found that the trend of increased melt rates under shrub canopy was generally, but not always, enhanced when compared to open tundra areas citing initial snow depth, shrub height, species, and bending of shrub canopy as variables affecting melt rates. High variability in shrub effects on localized snowmelt rates and basin melt patterns have created issues for current hydrological models limiting their ability to accurately predict the spatial distribution of snowmelt (Knox et al., 2012; Liston et al., 2002; Pohl and Marsh, 2006). Vegetation influences are further complicated by inconsistencies relating to the effects of shrub cover on snow accumulation and melt rates stemming from the bending of shrubs during the winter months (Sturm et al., 2001). Incorporating shrub bending into models has proven difficult (Essery and Pomeroy, 2004; Menard et al., 2014) and emphasizes the need for further research into high-resolution data-driven studies to address these complexities.

Spatial and temporal variations in snowmelt contributing areas can be expressed as a function of snow depth and the required cold content of a snowpack (DeBeer and Pomeroy, 2010; Pohl and Marsh, 2006; Pomeroy et al., 2006). The heterogeneous distribution in end-of-winter snow generally results in the melting of upland tundra areas first, followed later by deeper snow drifts, whereby the former contains a relatively small SWE and initial snow depth and subsequently tend to completely melt much earlier than the deeper snowpacks found on hillslopes (Marsh and Pomeroy, 1996; Quinton and Carey, 2008). Numerous studies have focused on understanding the spatial and temporal snowmelt patterns in tundra environments (Quinton and Marsh, 1999; Quinton *et al.*, 2004; Pohl *et al.*, 2006; Marsh *et al.*, 2008, 2010; Quinton and Carey, 2008; DeBeer and Pomeroy, 2010), however, our current ability to model and predict what

areas are actively melting, and what areas of the basin are actively contributing meltwater runoff to the streamflow at a given time are still poorly understood and further complicated by a warming climate.

Heterogenous snowmelt across the landscape causes spatial and temporal variations in snowmelt sourced runoff. Numerous studies focused on the temporal lag between melt production and runoff timing with a focus on modelling meltwater pathways through the basin (Marsh and Pomeroy, 1996; Marsh and Woo, 1981; Quinton and Marsh, 1998), however, many unknowns remain regarding water storage and contributing areas to runoff during the spring snowmelt. Quinton and Marsh (1998) examined meltwater fluxes and runoff pathways for a small tundra permafrost basin and found that initially vertical percolation occurs very slowly within the snowpack, but concluded that percolation time is rapid for hillslopes. Similarly, other studies have shown that large drifts do not contribute to runoff during the beginning of the melt season and instead store much of the early meltwater, which is then slowly released over the course of the melt period (DeBeer and Pomeroy, 2010; Marsh et al., 2008; Quinton and Marsh, 1999, 1998).

Previous research in Arctic tundra environments, as seen by Marsh *et al.*, (1995) for example, demonstrate the importance of accurate measurements the spring hydrological system as the spring freshet can account for upwards of 90% of the annual stream discharge. Hydrological datasets that address the spatial variations in snowcover over the rapid melt will provide researchers with a better understanding of the complex interactions between snow distribution, snowmelt patterns, and streamflow

response which will lead to improvement of our ability to predict and forecast these systems under future changes.

Snow measurements using remote sensing

Until very recently, the primary methods for measuring snow conditions across large scales applied the use of airborne or satellite based, applying a multitude of instruments and sensors to quantify snow cover conditions at a wide variety of spatial and temporal scales. Satellite-based remote sensing may provide information on snow on a large scale and does so with moderate accuracy. However, these large scale techniques often fail to capture the full heterogeneity of the snowcover and are severely limited in their temporal acquisitions; they are also very expensive to build and operate.

Current remote sensing techniques feature a multitude of spatial resolutions heavily dependant on the type of sensor and objectives of the satellite or airborne mission. Spatial resolutions often range from meter-sized ground sampling distances (resolution frequently desired for airborne lidar) to multiple kilometers (as seen with most satellite-based products). The following section provides a brief overview of the primary functions and applications of these two remote sensing techniques followed by a discussion of each method's pros and cons from a snow hydrology perspective.

Light Detection and Ranging (lidar) is a remote sensing technique used by hydrologists and remote sensing technicians to measure snow depths across a study area. Lidar measurements of snow depth can be undertaken using either ground-based laser scanning stations or airborne mounted laser scanners. For applications relating to this study only the latter will be discussed, but the methodologies are similar for both aerial and terrestrial lidar. Airborne lidar utilizes highly precise georeferenced elevation

maps obtained from an aircraft mounted lidar instrument referenced using an internal GPS and coupled Inertial Measurement Unit (IMU) or a high-precision ground-based GPS system. Snow depth is then determined by differentiating between co-registered lidar maps obtained 1) during a snow-free period (also referred to as the base map, or reference map), and 2) during a snow-covered period. Due to the high accuracy of the GPS georeferenced lidar maps, the airborne lidar technique is often able to quantify the snow depth with a sub-decimeter vertical accuracy, while covering spatial areas ranging from sub-kilometer squared to full basin extents (refer to Deems *et al.* (2013) for further review).

The lidar instrument is an active ranging instrument that measures the time-of-flight of a laser pulse allowing for the determination of the distance of travel between the scanner (aircraft) and the target (ground) (Deems et al., 2013). The position of the aircraft mounted sensor is determined using a high-precision GPS along with an internal IMU which determines the sensor platform roll, pitch, and yaw to establish the aircrafts, and thus sensors, geometry relative to the ground surface. Once the sensor and platform conditions are known the target distance (i.e. distance to ground/ surface elevation) is determined by measuring the time of travel for the laser pulse to return to the sensor. Uncertainties introduced here have the potential to affect the final accuracy of the lidar elevation estimates. Previous lidar sensors were only capable of providing discrete returns (one return signal) representing one single peak in the backscatter reflection of the surface. However new sensors can capture the entire back scatter illumination (full-wave lidar) which allows for a more accurate retrieval of surface elevations across multiple reflection environments (Mallet and Bretar, 2009) and allows

for the distinction between multiple surfaces such as vegetation heights, understory structure, and bare surface heights (Deems *et al.*, 2013).

Measuring snow depths using airborne lidar is well established in the literature and has proven successful for measure the snow depth across basin scales with high accuracy (Deems et al., 2013; Hedrick et al., 2015; Painter et al., 2016). However, measuring snow depths using lidar is not without flaw. First, a major limitation to airborne lidar is cost. Planning and executing an airborne lidar campaign requires expensive instrumentation and extensive personnel for manned aircraft flight and field validation campaigns. Secondly, the complexity of post-processing of raw lidar data requires specialized software and trained professional to produce the high-precision results. Thirdly, the use of airborne lidar, and the accuracy of results, are highly subject to weather patterns and atmospheric conditions, limiting data collection to clear, calm conditions. These conditions cannot always be met and can result in large delays, or failure, of a scheduled campaign. A final disadvantage of this method lies in the complexity estimating snow water equivalent from spatially distributed snow depths across a study area. Issues arise from the uncertainties with estimating spatial trends in snowpack density (Raleigh and Small, 2017) especially for complex or changing snowpacks.

Satellite-based remote sensing of snow can provide valuable information of snow cover extent and SWE dependant on the type of sensor onboard the satellite. These may include optical, active (synthetic aperture radar or SAR) or passive microwave sensors, with each sensor platform featuring specific applications for measuring various

snowpack conditions. A primary advantage of these methods is the large spatial coverage allowing for national or global-scale coverage.

Optical sensors capture specific wavelengths of the light spectrum, with bandwidth ranging from sensor to sensor. These sensors are primarily directed towards determining snow covered extent by analyzing the wavelengths for pixels covered by snow. Optical sensors such as those mounted on the Advanced Very High Resolution Radiometer (AVHRR), the Moderate Resolution Imaging Spectroradiometer (MODIS) and the Landsat series of satellites, to name a few, allow researchers to accurately determine snow cover extent at a regional to global scale. Snow cover is often easy to differentiate from bare ground because of the high portion of light in the visible spectrum that is reflected. The ability of snow to reflect light in the visible spectrum, also known as its albedo, is influenced greatly by the snowpacks grain size, age, and concentration of impurities (i.e. surface dust). Distinguishing between snow cover and cloud cover however is complicated as snow cover and clouds behave similarly in the reflective and thermal portions of the electromagnetic spectrum (Dietz et al., 2012).

Another issue with satellite-based optical sensors is the coarse spatial and temporal resolutions of data acquisition. For example, MODIS features daily snow cover products from its Aqua and Terra satellites, with a spatial resolution of 500 meters, while the Landsat +ETM and Landsat 8 products are available with a spatial resolution of 30 meters but feature a coarse temporal resolution of 16-18 days. The coarse spatial and temporal resolution can often result in large uncertainties estimating the fractional snow cover as snow melt does not occur heterogeneously across the majority of landscapes (Dietz et al., 2012; Salomonson and Appel, 2004) and further results in a failure to

capture small scale changes in regional snow cover, especially during the rapid snowmelt period. However, they do provide valuable information on large scale and global trends with great ease and high accuracy.

Passive microwave remote sensing relies on the principle that snow attenuates the naturally emitted microwave radiation from the Earth's surface, whereby an increased snowpack mass and thus increased ice and water content reduces the emitted microwave radiation that reaches the satellite sensor (Dietz *et al.* (2012) for a more detailed overview). The propagation of microwaves through a snowpack is affected by the dielectric constants of ice and water which vary greatly with properties such as liquid water content, grain size and shape (Dietz *et al.,* 2012). Passive microwave sensors apply a variety of wavelength frequencies and polarizations to map snow surface conditions, with each combination featuring specific benefits. For example, vertically polarized data are more sensitive to mapping snow volume and are useful for mapping shallow snowpacks, while horizontally polarized data are best suited for mapping snow cover (Dietz *et al.*, 2012). Frequency is also critical to passive microwave sensors as the frequency is responsible for the wavelength and spatial resolution of the signals, but the frequency also dictates the maximum snow depth that can be derived (Dietz *et al.*, 2012).

Passive microwave sensors are not only sensitive to the conditions of the snowpack, but also to vegetation cover which leads to errors in snow depth and SWE estimates as vegetation absorbs microwave radiation at a certain wavelengths suppressing the scattering surface (Dong, 2018). The presence of liquid water in the snowpack is also seen to increase the dielectric loss and increases absorption of

microwaves within the snowpack which can render passive microwave sensing useless once the snow begins to melt. The coarse resolution of passive microwave sensors allows for acquisition of global datasets at daily time steps, but this results in less than ideal conditions for measuring regional snow cover conditions, especially for regional water balance studies where an entire basin may be one or two pixels.

Active sensors emit energy to scan the Earth and measure the amount of radiation that is reflected (also known as backscatter) from the surface. Active sensors often apply radar (Radio Detection and Ranging) methods to measure the snow cover conditions. Lidar (Light Detection and Ranging) is also considered an active sensor and is commonly used method for mapping snow depth. Synthetic Aperture Radar (SAR) is used by most active satellite sensors (RADARSAT-2, TerraSAR-X, QuickSCAT to mention a few). Active sensors often feature a finer ground sampling resolution than passive microwave sensors, however unlike passive sensors active sensors do not work well over dry snowpacks making them ideal for measuring snow during the snowmelt (Dietz et al., 2012; Dong, 2018). Active remote sensing products feature higher resolution products when compared to passive remote sensing methods, but data acquisitions for these products are often very costly.

Unmanned Aerial Systems and photogrammetry

Recent advances in Unmanned Aerial Systems (UAS, commonly referred to as "drones") has enabled users to create high-resolution elevation and optical multi-wavelength imagery using *Structure-from-Motion* (SfM) photogrammetry software. There are many commercially available SfM photogrammetry software packages (Pix4D, Agisoft, ArcGIS drone-to-map etc.) but they all operate using similar principles.

16

The basis of photogrammetry lies in its ability to take 2-dimensional photographic representations and convert them into 3-dimensional objects in space. SfM photogrammetric software joins together digital aerial photographs captured from the UAS and georeferenced during a flight using an onboard GPS system and a combination of reference ground control points (GCPs). By triangulating common tie points in multiple images the software is able to create a 3-dimensional point cloud, assigning an X, Y and Z coordinates to each pixel. The output products of SfM photogrammetry include orthorectified aerial mosaics of the study site and a 3-dimensional point cloud which can be converted into a Digital Surface elevation Model (DSM). SfM photogrammetry can produce spatial datasets with a point cloud density and accuracy comparable, if not finer, to those generated by the lidar methods described above.

One of the first papers to demonstrate the SfM technique for mapping snow depths was Nolan *et al.* (2015). In their study, Nolan *et al.*, (2015) applied SfM photogrammetry over large areas using a consumer-grade camera mounted to the base of a manned aircraft. The study applied SfM snow depth mapping at three locations in Alaska and showed the snow depth products produced using this technique were statistically similar to the actual snow on the ground to ±10 cm once known sources of error were removed. This study demonstrated the effectiveness and accuracy of the SfM photogrammetry technique for measuring centimeter-level change detection that provides an affordable and effective remote sensing method for mapping snow at landscape scales. Although this study utilized a manned aircraft the same procedures and processing steps are followed when using unmanned aircraft.

UAS platforms often take the form of fixed-wing aircraft or multi-rotor copters (Quad-copter, Octo-copter, etc.). There are many benefits and trade-offs between the two, but the main difference lies in the spatial coverage and output ground sampling distance (GSD) resolution. A rapid rise in UAS technology in scientific literature has occurred in recent years, particularly in the field of snow hydrology as the ability to create high-resolution snow depth products are well suited for capturing spatial variation in snow cover.

In recent years, there has been a surge in studies utilizing SfM photogrammetry and Unmanned Aerial for mapping snow depth in prairie and alpine environments (Bühler et al., 2016; Bühler et al., 2017, 2015; De Michele et al., 2016; Harder et al., 2016; Vander Jagt et al., 2015). These studies have demonstrated strong, although variable, success for measuring snow depth, with strong agreement between UAS and in-situ observation. The technique applied is identical to mapping snow depths using airborne lidar, except the surface elevations are derived from the GPS positioning of each images captured during flight, and then georeferenced during the processing stage using a high-precision GPS (<0.05 m) and previously deployed ground control points (GCPs). These studies mark the advent of a valuable tool for creating high-resolution spatial datasets and signals a new wave of remote sensing products that bridges the scale gap between point observations collected in the field and coarse-resolution satellite-based products.

Applications of Unmanned Aerial Systems for documenting landscape-scale snowcover properties is still novel, and the experimental nature of this technique has revealed mixed results across the few existing studies. As a result, the current literature,

18

although rapidly expanding, is limited in nature. This is especially the case as no study

to date has applied SfM snow depth mapping in heavily vegetated regions. The current

literature is also limited in that all existing studies were either conducted across prairie

or alpine regions featuring little to no vegetation to influence the results. The current

literature is also mixed when it comes to study design and validation accuracy. For

example, Vander Jagt *et al.* (2015) presented one of the first application of UAS

mapping of snow depths for an alpine environment using a quad-copter style UAV and

revealed an estimated snow depth error of roughly 10 cm. However, this study was

conducted over a very small area (0.007 km^2) and only featured 20 in-situ snow depth

validation points. Other studies, such as De Michele *et al.* (2016), Bühler *et al.* (2015,

2017), and Bühler *et al.* (2016) also applied a similar method for mapping snow depth in

alpine environments, with estimated snow depth errors of 14 cm, 30 cm, 17-23 cm, and

7-15 cm respectively. Unfortunately, due to the experimental nature of this new

technique, the small aerial coverage and relatively simplistic validation techniques, at

least relating to in-situ snow depths, limit the effective validation of the technique. For

example, De Michele *et al.* (2016) demonstrated a strong RMSE of 14 cm between

observed and UAS derived snow depths, however the study only featured 12 ground

validation points for the homogenous 0.3 km^2 area covered by the fixed-wing UAS.

Arguably the strongest application of UAS photogrammetry for measuring snow depth

was conducted by Harder *et al.* (2016) using a real-time Kinematic GPS (RTK) fixed-

wing UAS over sparsely vegetated prairie (0.65 km^2) and alpine (0.32 km^2) landscapes.

This study demonstrated mixed results for various land cover types and demonstrated

that vegetation does have a negative impact on the overall accuracy of the UAS derived

snow depths (RMSE vary from 8.8 cm to 13.7 cm due to height differences of prairie stubble influences). This study also demonstrated the first application of successful change detection due to snowpack ablation and highlights key environmental conditions that may affect the accuracy of UAS methods.

To the authors knowledge, no SfM-based applications of snow depth have produced estimates of SWE to date. This is due to difficulties interpolating snow density across a landscape (Raleigh and Small, 2017). Furthermore, no study to date has continually assessed the changes in snow depth or SWE across an entire spring snowmelt period using the above described methods. This study attempts to address these gaps in the literature by applying UAS measurements of snow covered area, SWE, and melt rates across the spring melt at high spatial and temporal resolutions. This will enable direct measurements useful for assessing spatial heterogeneity in snowmelt patterns and quantifying changes to the basin hydrology over the melt.

Knowledge Gaps

Predicting and forecasting changes to the hydrologic regimes of Arctic environment resulting from continued climate warming highlights uncertainty towards how these systems will respond and change in the future. Temperature increases, especially during the spring period, will have great impacts on the spring melt timing and magnitude of freshet runoff, resulting in an earlier spring melt dates and expediated melt timings (Foster et al., 2008; IPCC, 2013; Overland et al., 2004; Shi et al., 2015). However, a recent study by Shi *et al.* (2015) concluded increased spring air temperatures were associated with a delayed streamflow runoff for an Arctic tundra catchment suggesting complex and poorly understood interactions between climate,

hydrology and other aspects of the physical environments. This study is among others (Musselman et al., 2017) that cite a need for the further understanding of the physical interactions among the many complexities that influence the changes to the spring hydrological regimes of these environments.

Contradictory changes to the hydrological regimes of tundra systems from changes in climatic conditions highlight knowledge gaps relating to interactions of physical processes during the spring snowmelt and freshet. The complexities, often associated with quantifying spatial distributions in end-of-winter snowcover and changes to the snowpack over the spring melt, result in a poor understanding of snow storage and meltwater available to the hydrological system. The main issue lies in difficulties measuring snow precipitation while simultaneously capturing spatial distributions of SWE across various land cover types at basin scales. Traditionally, this has been an issue of bridging the gap between point-scale measurements of precipitation using meteorological instruments, point measurements of snow on the ground, and coarse-resolution remote sensing estimates of SWE and snowpack characteristics. Furthermore, measuring changes to the hydrological systems are further complicated by a lack of high-resolution data on snow distribution, snowmelt patterns and melt rates resulting in an inability to accurately capture micro-scale changes to the tundra snow cover.

A final uncertainty cites the need for comprehensive hydro-meteorological datasets to validate and improve available hydrological models to be able to better forecast future changes to the systems (Clark et al., 2017). At present, the heterogeneous nature of the end-of-winter snowcover and complex snowmelt

processes provide uncertainties in modelling the spring snowmelt and corresponding freshet. If current hydrological models can not accurately reproduce the current conditions at high resolutions how are they expected to be able to model these systems under future climate change conditions? Uncertainties here arise from complex physical processes relating to quantifying and better parameterizing; blowing snow and sublimation over the winter, spatial changes in snowpack density, accurate end-of-winter snow distribution at small scale resolutions, meltwater runoff, snowmelt contributing areas, impacts of vegetation of snowmelt timing, and the effects of snow and ice dams within the channels. It is hopeful that increases in computational power allowing for high-resolution spatially-distributed hydrological models will address these issues. To address such issues, current literature in the hydrological modelling community is pushing towards the creation and integration of improved high-resolution comprehensive datasets that will allow for further improvement our understanding of physical processes and models (Peters-Lidard et al., 2017). Advances in remote sensing platforms, as such with the advent of Unmanned Aerial Systems, and increased long-term hydro-meteorological datasets will contribute to improving high-resolution documentation of snowcover conditions and predictions of the spring freshet under further changing environmental conditions.

Conclusion

Tundra snow characteristics have been well researched since the 1970's and as a result a large amount of literature exists focused on late winter snowpack conditions for these environments. Unfortunately, little research has focussed on understanding the spring snowmelt patterns to understand small-scale heterogeneity of snow

conditions across the melt. Further research is needed to better understand the dynamics of such systems as they account for such a substantial portion of the total annual stream discharge and the timing and magnitude of meltwater runoff strongly influences the spring freshet- the most hydrologically important event in Arctic tundra environments. Advances in complex high-resolution spatially distributed hydrological models have proven ineffective at accurately modelling snow in tundra environments, and further fail to capture the spring snowmelt patterns. This is partially a result of models' inability to accurately represent small-scale heterogeneity at multiple scales by these physical-based hydrological models. A push towards such models therefore requires corresponding high-resolution hydro-meteorological datasets to validate the model products and to improve the accuracy of the models ability to represent heterogeneity across all scales (Sivapalan, 2018). With the advent of novel technological advances, particularly through the arrival of UAS remote sensing of snow techniques, such high-resolution datasets to validate landscape scale snow cover are now possible, although little work to date has successfully applied this technology across changing snow cover conditions during the spring melt. This research, combined with comprehensive long-term hydro-meteorological datasets, should help increase the accuracy of hydrological models and better understand how a changing climate will affect tundra streamflow regimes.

Research Objectives and Study Site

Research motivation

Dramatic increases in global surface temperatures have been well documented in recent decades (IPCC, 2013), with temperatures in polar environments increasing at

over double the rate of the global average, and without dramatic decreases in carbon emissions, temperatures will continue to rise drastically. As the climate warms and precipitation patterns change, there will be significant impacts on the hydrological cycle of northern tundra environments, but the cumulative effects on these systems are still uncertain. Standard snow survey methods, and low-resolution remote sensing methods that are normally used in most Arctic snowmelt studies to date, can not accurately measure fine-scale spatial heterogeneity in snowcover and snowmelt in these environments. We believe that this limits our ability to predict and forecast hydrological regimes under a changing climate, including changes in precipitation, vegetation and permafrost. This research attempts to provide a better understanding of these complex hydrological systems through the infilling of knowledge gaps relating to spatio-temporal changes in Arctic tundra snow cover and snowmelt patterns to contribute to the future improvement of hydrological models.

Research questions

This thesis aims to address the following research questions:

1. How does micro-scale variability in snow covered area and snow water equivalent vary over the melt period?

2. What is the influence of land cover type on the timing of snowmelt, and how does this vary across the melt period?

Objectives

The primary objective of this study is to better understand micro-scale changes to the snowpack over the spring snowmelt period. Specifically, this thesis will focus on

documenting the spatio-temporal variability in snowpack conditions of an Arctic tundra headwater catchment to provide direct observations of snow covered area, water equivalent and melt rates over the melt. Few studies to date have successfully demonstrated the ability to map snow water equivalent at catchment scales, with even fewer studies mapping SWE over Arctic tundra catchments. The result is a lack of data driven science about high-resolution spatial distributions of snow leading to a lack of understanding of spring snowmelt regimes and the relation to the hydrologically important spring freshet. This thesis attempts to address these issues through high-resolution remote sensing analysis of basin distributed snowcover conditions during the melt. Going forward, these data-driven observations may be coupled with traditional hydrological methods such as snow surveys, eddy covariance, and streamflow measurements resulting in the creation of high-resolution datasets suited towards integration with future high-resolution spatially distributed hydrological models.

Objective 1: Develop a methodology to quantify micro-scale snow water equivalent across the snowmelt period using Unmanned Aerial Systems (UAS).

Objective 2: Quantify the spatial and temporal variability in snow conditions over the snowmelt, with a focus on changes in SCA and SWE across various land cover types.

Study site

Siksik Creek (68.74N, -133.49W), a 95-hectare sub-catchment of Trail Valley Creek (Figure 1-1), lies in the southern Tuktoyaktuk Coastal Plains located east of the Mackenzie Delta within the Inuvialuit Settlement Region. The small headwater basin drains south into Trail Valley Creek, which then flows north towards the Arctic Ocean

through the Eskimo Lakes estuary (commonly referred to as *Husky Lakes*). The basin is situated 50 kilometers north-north east of Inuvik and 75 km south of Tuktoyaktuk.

Siksik Creek is located in a region of ice-rich continuous permafrost that is approximately 150-350 meters in depth (Heginbottom and Radburn, 1992), and has active-layer depths ranging from 30 to 120 centimeters. This study site is located along the northern fringe of the forest-tundra ecozone with vegetation dominated by grasses, lichen, and mosses with low-lying (birch) and tall (willow and alder) shrubs and small isolated patches of black spruce trees. The topography consists of gently rolling hills, with elevations in the Siksik Creek basin ranging between 60 to 100 meters above MSL. Characteristics of this small basin are similar to those of the larger Trail Valley Creek basin, however the Siksik catchment does not feature lakes or spruce forest patches.

The climate of this region is characterized by short, cool summers and long, cold winters. Meteorological data has been collected since the early 1990s at the Trail Valley Creek Main Meteorological station (TMM) and by Environment and Climate Change Canada (ECCC) since 1999. ECCC climate normals for nearby *Inuvik A* meteorological station reveal an annual average temperature of -8.2°C and 240 mm of annual precipitation (Environment and Climate Change Canada, 2018) (refer to Appendix 1a). However, there is a strong gradient in temperature and precipitation between Inuvik and Tuktoyaktuk which features a mean annual temperature of -10.2°C and 139 mm total precipitation (Appendix 1b). The climate at TMM is expected to fall between the normal of these two long term stations. Much of the annual precipitation falls between late August and October with rain dominating the August-September period and snow in

October, although snow can fall at any time of the year. Approximately 66 percent of the annual precipitation falls as snow in this basin (Mann, 2018).

The spring snowmelt typically begins in mid-to-late May. This period is marked by temperature increases above 0°C and increased incoming solar radiation which results in the rapid melt of the snow and the rise of the spring freshet hydrograph. The distribution of the winter snowfall is heterogeneous in nature with large amounts of snow stored in large hillslope and channel drifts (> 185cm depth) that cover approximately 6% of the Siksik basin and 17% of the Trail Valley Creek basin area (Pomeroy et al., 1997; Quinton and Marsh, 1998). Significant variations of snow across the landscape in the form of snow drifts are important because they store a relatively large portion of the snow and contribute meltwater runoff to the hydrological systems late into the spring season.

The Siksik Creek hydrograph is predominantly driven by the release of stored winter snow during the spring snowmelt period. Nearly 90 percent of the annual discharge occurs during this short spring freshet period (Marsh et al., 1995) due to the impermeability of the underlying permafrost during the spring snowmelt periods which provide little soil storage for runoff (Quinton and Marsh, 1999, 1998). After the spring freshet, streamflow is dominated by rainfall precipitation events and released groundwater stored in the ice-rich soils as the active layer begins to develop releasing stored water from the previous year.
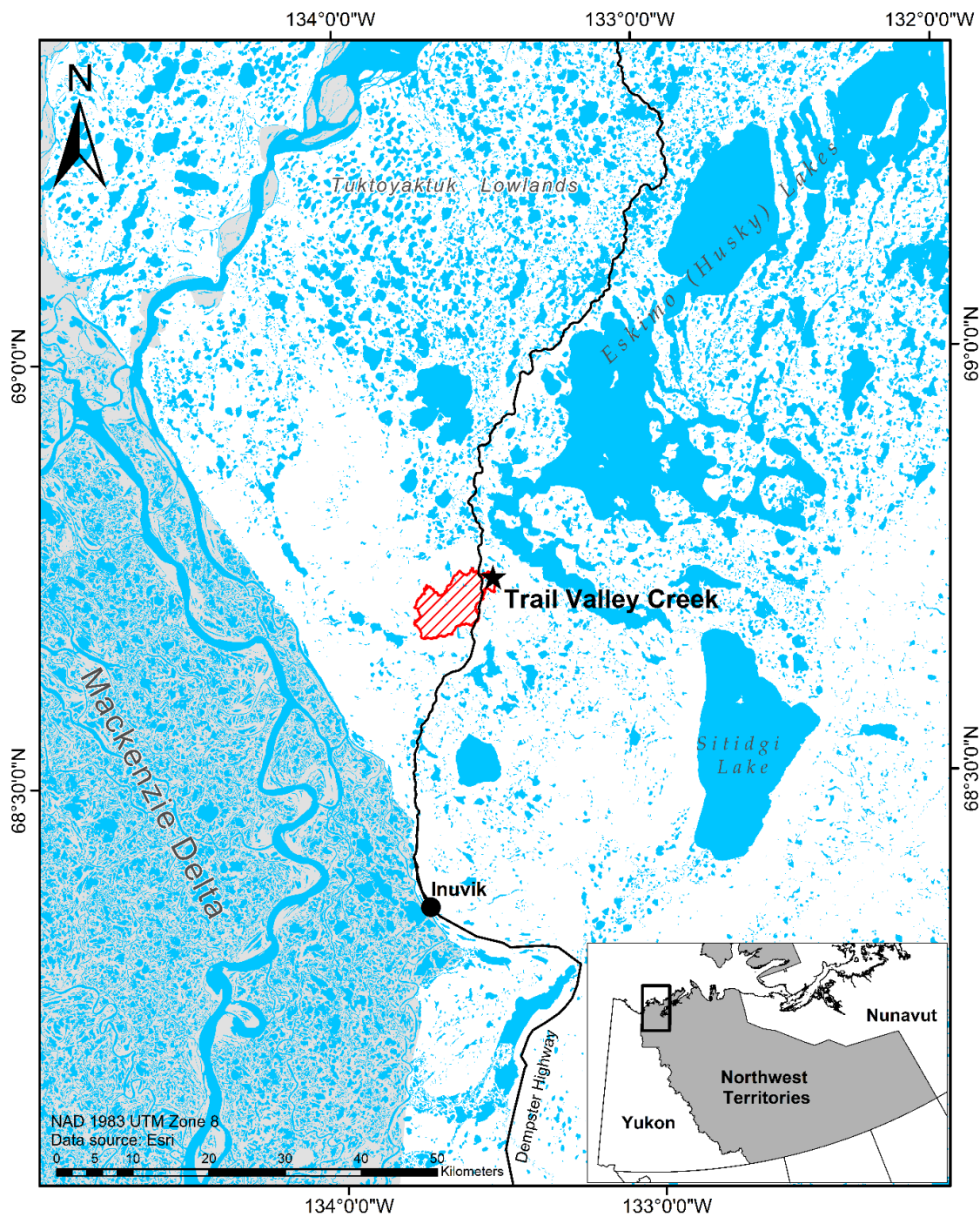
Figure 1-1: Trail Valley Creek, NWT is located 50 kilometers north of Inuvik between the Inuvik-Tuktoyaktuk Highway and the Eskimo (Husky) Lakes system. Red polygon delineates the watershed boundary upstream of the Water Survey of Canada stream gauge.

References

Bring, A., Fedorova, I., Dibike, Y., Hinzman, L., Mård, J., Mernild, S.H., Prowse, T., Semenova, O., Stuefer, S.L., Woo, M.K., 2016. Arctic terrestrial hydrology: A synthesis of processes, regional effects, and research challenges. J. Geophys. Res. G Biogeosciences 121, 621–649. https://doi.org/10.1002/2015JG003131

Bühler, Y., Adams, M.S., Bosch, R., Stoffel, A., 2016. Mapping snow depth in alpine terrain with unmanned aerial systems (UASs): Potential and limitations. Cryosphere 10, 1075–1088. https://doi.org/10.5194/tc-10-1075-2016

Bühler, Y., Adams, M.S., Stoffel, A., Boesch, R., 2017. Photogrammetric reconstruction of homogenous snow surfaces in alpine terrain applying near-infrared UAS imagery. Int. J. Remote Sens. 38, 3135–3158. https://doi.org/10.1080/01431161.2016.1275060

Bühler, Y., Marty, M., Egli, L., Veitinger, J., Jonas, T., Thee, P., Ginzler, C., 2015. Snow depth mapping in high-alpine catchments using digital photogrammetry. Cryosphere 9. https://doi.org/10.5194/tc-9-229-2015

Clark, M.P., Bierkens, M.F.P., Samaniego, L., Woods, R.A., Uijlenhoet, R., Bennett, K.E., Pauwels, V.R.N., Cai, X., Wood, A.W., Peters-Lidard, C.D., 2017. The evolution of process-based hydrologic models: Historical challenges and the collective quest for physical realism. Hydrol. Earth Syst. Sci. 21, 3427–3440. https://doi.org/10.5194/hess-21-3427-2017

Colbeck, S.C., 1982. An overview of seasonal snow metamorphism. Rev. Geophys. 20, 45. https://doi.org/10.1029/RG020i001p00045

Colbeck, S.C., 1979. Grain clusters in wet snow. J. Colloid Interface Sci. 72, 371–384. https://doi.org/10.1016/0021-9797(79)90340-0

De Michele, C., Avanzi, F., Passoni, D., Barzaghi, R., Pinto, L., Dosso, P., Ghezzi, A., Gianatti, R., Vedova, G. Della, 2016. Using a fixed-wing UAS to map snow depth distribution: An evaluation at peak accumulation. Cryosphere 10, 511–522. https://doi.org/10.5194/tc-10-511-2016

DeBeer, C.M., Pomeroy, J.W., 2010. Simulation of the snowmelt runoff contributing area in a small alpine basin. Hydrol. Earth Syst. Sci. 14, 1205–1219. https://doi.org/10.5194/hess-14-1205-2010

Deems, J.S., Painter, T.H., Finnegan, D.C., 2013. Lidar measurement of snow depth: A review. J. Glaciol. 59, 467–479. https://doi.org/10.3189/2013JoG12J154

Dietz, A.J., Kuenzer, C., Gessner, U., Dech, S., 2012. Remote sensing of snow – a review of available methods. Int. J. Remote Sens. 33, 4094–4134. https://doi.org/10.1080/01431161.2011.640964

Dong, C., 2018. Remote sensing, hydrological modeling and in situ observations in snow cover research: A review. J. Hydrol. 561, 573–583. https://doi.org/10.1016/j.jhydrol.2018.04.027

Environment and Climate Change Canada, 2018. Canadian Climate Normals 1981-2010 Station Data: Inuvik A [WWW Document]. URL http://climate.weather.gc.ca/climate_normals/results_1981_2010_e.html?stnID=1669&autofwd=1 (accessed 7.12.18).

Essery, R., Pomeroy, J., 2004. Vegetation and Topographic Control of Wind-Blown Snow Distributions in Distributed and Aggregated Simulations for an Arctic Tundra Basin. J. Hydrometeorol. 5, 735–744. https://doi.org/10.1175/1525-7541(2004)005<0735:VATCOW>2.0.CO;2

Foster, J.L., Robinson, D. a., Hall, D.K., Estilow, T.W., 2008. Spring snow melt timing and changes over Arctic lands. Polar Geogr. 31, 145–157. https://doi.org/10.1080/10889370802580185

Goodison, B., Louie, P.Y.T., Yang, D., 1998. WMO solid precipitation measurement intercomparison. Final Rep. 318.

Harder, P., Schirmer, M., Pomeroy, J., Helgason, W., 2016. Accuracy of snow depth estimation in mountain and prairie environments by an unmanned aerial vehicle. Cryosphere 10, 2559–2571. https://doi.org/10.5194/tc-10-2559-2016

Hedrick, A., Marshall, H.P., Winstral, A., Elder, K., Yueh, S., Cline, D., 2015. Independent evaluation of the SNODAS snow depth product using regional-scale lidar-derived measurements. Cryosphere 9, 13–23. https://doi.org/10.5194/tc-9-13-2015

Heginbottom, J.A., Radburn, L.K., 1992. Permafrost and ground ice conditions of northwestern Canada; Geological Survey of Canada, Map 1691A, scale 1:1,000,000.

Helgason, W.D., Pomeroy, J.W., 2005. Uncertainties in Estimating Turbulent Fluxes to Melting Snow in a Mountain Clearing. 62nd East. Snow Conf. 129–142.

IPCC, 2013. Observations: Atmosphere and surface, Climate Change 2013: The Physical Science Basis. Contribution of Working Group I to the Fifth Assessment Report of the Intergovernmental Panel on Climate Change. Cambridge University Press, Cambridge, United Kingdom and New York, NY, USA. https://doi.org/10.1017/CBO9781107415324.008

Kane, D.L., Hinzman, L.D., Benson, C.S., Liston, G.E., 1991. Snow hydrology of a headwater Arctic basin 1. Physical measurements and process studies. Water Resour. Res. 27, 1099–1109.

Knox, S.H., Carey, S.K., Humphreys, E.R., 2012. Snow surface energy exchanges and snowmelt in a shrub-covered bog in eastern Ontario, Canada. Hydrol. Process. 26, 1877–1891. https://doi.org/10.1002/hyp.9289

Kokelj, S. V, Burn, C.R., 2005. Geochemistry of the active layer and near-surface permafrost, Mackenzie delta region, Northwest Territories, Canada. Can. J. Earth Sci. 42, 37–48. https://doi.org/10.1139/E04-089

Lantz, T.C., Gergel, S.E., Kokelj, S. V., 2010. Spatial heterogeneity in the shrub tundra ecotone in the Mackenzie Delta region, Northwest territories: Implications for Arctic environmental change. Ecosystems 13, 194–204. https://doi.org/10.1007/s10021-009-9310-0

Lantz, T.C., Marsh, P., Kokelj, S. V., 2013. Recent Shrub Proliferation in the Mackenzie Delta Uplands and Microclimatic Implications. Ecosystems 16, 47–59. https://doi.org/10.1007/s10021-012-9595-2

Liston, G.E., Mcfadden, J.P., Sturm, M., Pielke, R. a, 2002. Modelled changes in arctic tundra snow, energy and moisture fluxes due to increased shrubs. Glob. Chang. Biol. 8, 17–32. https://doi.org/10.1046/j.1354-1013.2001.00416.x

Macdonald, J., Pomeroy, J., 2007. Gauge Undercatch of Two Common Snowfall Gauges in a Prairie Environment. Proc. 64th East. Snow Conf. St. John's, Canada. 119–126.

Mallet, C., Bretar, F., 2009. Full-waveform topographic lidar: State-of-the-art. ISPRS J. Photogramm. Remote Sens. 64, 1–16. https://doi.org/10.1016/j.isprsjprs.2008.09.007

Mann, P., 2018. Spatial and temporal variability of the snow environment in the Western Canadian Arctic. Wilfrid Laurier University.

Marsh, P., 1987. Grain growth in a wet arctic snow cover. Cold Reg. Sci. Technol. 14, 23–31. https://doi.org/10.1016/0165-232X(87)90041-3

Marsh, P., Bartlett, P., MacKay, M., Pohl, S., Lantz, T., 2010. Snowmelt energetics at a shrub tundra site in the western Canadian Arctic. Hydrol. Process. 24, 3603–3620. https://doi.org/10.1002/hyp.7786

Marsh, P., J. Pomeroy, S. Pohl, W. Quinton, C. Onclin, M. Russell, N. Neumann, A. Pietroniro, B. Davison, S. McCartney, 2008. Snowmelt processes and runoff at the Arctic treeline: Ten years of MAGS Research. Cold Reg. Atmos. Hydrol. Stud. Mackenzie GEWEX Exp. Volume 2:, 97–124.

Marsh, P., Pomeroy, J.W., 1996. Meltwater fluxes at an arctic forest-tundra site. Hydrol. Process. 10, 1383–1400. https://doi.org/10.1002/(SICI)1099-1085(199610)10:10<1383::AID-HYP468>3.0.CO;2-W

Marsh, P., Quinton, W.L., Pomeroy, J.W., 1995. Hydrological Processes and Runoff at the Arctic Treeline in Northwestern Canada. 10th Annu. North. Basins Symp. 368–397.

Marsh, P., Woo, M.-K., 1984. Wetting Front Advance and Freezing of Meltwater Within a Snow Cover 1. Observations in the Canadian Arctic. Water Resour. Res. 20, 1853–1864.

Marsh, P., Woo, M., 1981. Snowmelt, glacier melt, and high arctic streamflow regimes. Can. J. Earth Sci. 18, 1380–1384. https://doi.org/10.1139/e81-127

Menard, C.B., Essery, R., Pomeroy, J., Marsh, P., Clark, D.B., 2014. A shrub bending model to calculate the albedo of shrub-tundra. Hydrol. Process. 28, 341–351. https://doi.org/10.1002/hyp.9582

Mielko, C., Woo, M.K., 2006. Snowmelt runoff processes in a headwater lake and its catchment, subarctic Canadian Shield. Hydrol. Process. 20, 987–1000. https://doi.org/10.1002/hyp.6117

Musselman, K.N., Clark, M.P., Liu, C., Ikeda, K., Rasmussen, R., 2017. Slower snowmelt in a warmer world. Nat. Clim. Chang. 7, 214–219. https://doi.org/10.1038/nclimate3225

Nolan, M., Larsen, C., Sturm, M., 2015. Mapping snow-depth from manned-aircraft on landscape scales at centimeter resolution using Structure-from-Motion photogrammetry. Cryosph. Discuss. 9, 333–381. https://doi.org/10.5194/tcd-9-333-2015

O'Neill, H.B., Burn, C.R., 2016. Talik Formation at a Snow Fence in Continuous Permafrost, Western Arctic Canada. Permafr. Periglac. Process. 565, 558–565. https://doi.org/10.1002/ppp.1905

Overland, J.E., Spillane, M.C., Percival, D.B., Wang, M., Mofjeld, H.O., 2004. Seasonal and regional variation of pan-Arctic surface air temperature over the instrumental record. J. Clim. 17, 3263–3282. https://doi.org/10.1175/1520-0442(2004)017<3263:SARVOP>2.0.CO;2

Painter, T.H., Berisford, D.F., Boardman, J.W., Bormann, K.J., Deems, J.S., Gehrke, F., Hedrick, A., Joyce, M., Laidlaw, R., Marks, D., Mattmann, C., McGurk, B., Ramirez, P., Richardson, M., Skiles, S.M.K., Seidel, F.C., Winstral, A., 2016. The Airborne Snow Observatory: Fusion of scanning lidar, imaging spectrometer, and physically-based modeling for mapping snow water equivalent and snow albedo. Remote Sens. Environ. 184, 139–152. https://doi.org/10.1016/j.rse.2016.06.018

Pan, X., Yang, D., Li, Y., Barr, A., Helgason, W., Hayashi, M., Marsh, P., Pomeroy, J., Janowicz, R.J., 2016. Bias corrections of precipitation measurements across experimental sites in different ecoclimatic regions of western Canada. Cryosphere 10, 2347–2360. https://doi.org/10.5194/tc-10-2347-2016

Peters-Lidard, C.D., Clark, M., Samaniego, L., Verhoest, N.E.C., Van Emmerik, T., Uijlenhoet, R., Achieng, K., Franz, T.E., Woods, R., 2017. Scaling, similarity, and the fourth paradigm for hydrology. Hydrol. Earth Syst. Sci. 21, 3701–3713. https://doi.org/10.5194/hess-21-3701-2017

Pohl, S., Marsh, P., Liston, G.E., 2006. Spatial-temporal variability in turbulent fluxes during spring snowmelt. Arctic, Antarct. Alp. Res. 38, 136–146.

Pomeroy, J.W., Bewley, D.S., Essery, R.L.H., Hedstrom, N.R., Link, T., Granger, R.J., Sicart, J.E., Ellis, C.R., Janowicz, J.R., 2006. Shrub tundra snowmelt. Hydrol. Process. 20, 923–941. https://doi.org/10.1002/hyp.6124

Pomeroy, J.W., Essery, R.L.H., 1999. Turbulent fluxes during blowing snow: Field tests of model sublimation predictions. Hydrol. Process. 13, 2963–2975. https://doi.org/10.1002/(SICI)1099-1085(19991230)13:18<2963::AID-HYP11>3.0.CO;2-9

Pomeroy, J.W., Gray, D.M., 1995. Snowcover accumulation, relocation and management, National Hydrological Research Institute Science Report No. 7. Saskatoon.

Pomeroy, J.W., Marsh, P., D.M. Gray, 1997. Application of a distributed blowing snow model to the Arctic. Hydrol. Process. 11, 1451–1464. https://doi.org/10.1002/(SICI)1099-1085(199709)11:11<1451::AID-HYP449>3.0.CO;2-Q

Pomeroy, J.W., Schmidt, R.A., 1993. The use of fractal geometry in modelling intercepted snow accumulation and sublimation. 50th East. Snow Conf. 8-10 June 1993 1–10.

Prowse, T., Ommanney, S., 1990. Northern hydrology: Canadian perspectives. Environment Canada.

Quinton, W.L., Carey, S.K., 2008. Towards an energy-based runoff generation theory for tundra landscapes. Hydrol. Process. 22, 4649–4653. https://doi.org/10.1002/hyp.7164

Quinton, W.L., Carey, S.K., Goeller, N.T., 2004. Snowmelt runoff from northern alpine tundra hillslopes: major processes and methods of simulation. Hydrol. Earth Syst. Sci. 8, 877–890. https://doi.org/10.5194/hess-8-877-2004

Quinton, W.L., Marsh, P., 1999. A conceptual framework for runoff generation in a permafrost environment. Hydrol. Process. 13, 2563–2581. https://doi.org/10.1002/(SICI)1099-1085(199911)13:16<2563::AID-HYP942>3.0.CO;2-D

Quinton, W.L., Marsh, P., 1998. Meltwater fluxes, hillslope runoff and stream flow on an arctic permafrost basin. Permafrost, - 7th Int. Conf. Yellowknife (Canada), Collect. Nord. 921–926.

Raleigh, M.S., Small, E.E., 2017. Snowpack density modeling is the primary source of uncertainty when mapping basin-wide SWE with lidar. Geophys. Res. Lett. 44, 3700–3709. https://doi.org/10.1002/2016GL071999

Rees, A., English, M., Derksen, C., Toose, P., Silis, A., 2014. Observations of late winter Canadian tundra snow cover properties. Hydrol. Process. 28, 3962–3977. https://doi.org/10.1002/hyp.9931

Salomonson, V.., Appel, I., 2004. Estimating fractional snow cover from MODIS using the normalized difference snow index. Remote Sens. Environ. 89, 351–360. https://doi.org/10.1016/j.rse.2003.10.016

Shi, X., Marsh, P., Yang, D., 2015. Warming spring air temperatures, but delayed spring streamflow in an Arctic headwater basin. Environ. Res. Lett. 10, 064003. https://doi.org/10.1088/1748-9326/10/6/064003

Sivapalan, M., 2018. From engineering hydrology to Earth system science: Milestones in the transformation of hydrologic science. Hydrol. Earth Syst. Sci. 22, 1665–1693. https://doi.org/10.5194/hess-22-1665-2018

Sturm, M., Douglas, T., Racine, C., Liston, G.E., 2005. Changing snow and shrub conditions affect albedo with global implications. J. Geophys. Res. 110, G01004. https://doi.org/10.1029/2005JG000013

Sturm, M., McFadden, J.P., Liston, G.E., Stuart Chapin, F., Racine, C.H., Holmgren, J., 2001. Snow-shrub interactions in Arctic Tundra: A hypothesis with climatic implications. J. Clim. 14, 336–344. https://doi.org/10.1175/1520-0442(2001)014<0336:SSIIAT>2.0.CO;2

Thériault, J.M., Rasmussen, R., Ikeda, K., Landolt, S., 2012. Dependence of snow gauge collection efficiency on snowflake characteristics. J. Appl. Meteorol. Climatol. 51, 745–762. https://doi.org/10.1175/JAMC-D-11-0116.1

Vander Jagt, B., Lucieer, A., Wallace, L., Turner, D., Durand, M., 2015. Snow Depth Retrieval with UAS Using Photogrammetric Techniques. Geosciences 5, 264–285. https://doi.org/10.3390/geosciences5030264

Waldner, P. a., Schneebeli, M., Schultze-Zimmermann, U., Flühler, H., 2004. Effect of snow structure on water flow and solute transport. Hydrol. Process. 18, 1271–1290. https://doi.org/10.1002/hyp.1401

Whittington, P., Ketcheson, S., Price, J., Richardson, M., Di Febo, A., 2012. Areal differentiation of snow accumulation and melt between peatland types in the James Bay Lowland. Hydrol. Process. 26, 2663–2671. https://doi.org/10.1002/hyp.9414

Yang, D., Kane, D., Zhang, Z., Legates, D., Goodison, B., 2005. Bias corrections of long-term (1973-2004) daily precipitation data over the northern regions. Geophys. Res. Lett. 32, 1–5. https://doi.org/10.1029/2005GL024057

Young, K.L., Robert Bolton, W., Killingtveit, Å., Yang, D., 2006. Assessment of precipitation and snowcover in northern research basins. Nord. Hydrol. 37, 377. https://doi.org/10.2166/nh.2006.021

Chapter 2 : High resolution spatial variability in spring snowmelt in an Arctic tundra watershed

Authors:

Branden Walker[1], Philip Marsh[1]
[1] Cold Regions Research Centre, Wilfrid Laurier University. Waterloo, ON

Abstract

Arctic tundra environments are characterized by spatially heterogeneous end-of-winter snow cover because of high winds that erode, transport and deposit snow over the winter. This spatially variable end-of-winter snow cover subsequently influences the spatial and temporal variability of snowmelt and results in a patchy snowcover over the melt period. Documenting changes in both snow cover area (SCA) and snow water equivalent (SWE) during the spring melt is essential for understanding hydrological systems, but the lack of high-resolution SCA and SWE datasets that accurately capture micro-scale changes are not commonly available, and do not exist for the Canadian Arctic. This study applies high-resolution remote sensing measurements of SCA and SWE using a fixed-wing Unmanned Aerial System (UAS) to document snowcover changes over the snowmelt period for an Arctic tundra headwater catchment. Repeat measurements of SWE and SCA were obtained for four dominant land cover types (tundra, short shrub, tall shrub, and topographic drift) to provide observations of spatially distributed snowmelt patterns and basin-wide declines in SWE. High-resolution analysis of snowcover conditions over the melt reveal a strong relationship between land cover type, snow distribution, and snow ablation rates whereby shallow snowpacks found in tundra and short shrub regions feature rapid declines in SWE and SCA and became snow-free approximately 10 days earlier than deeper snowpacks. In contrast, tall shrub patches and topographic drift regions were characterized by large initial SWE values and featured a slow decline in SCA. Analysis of basin-wide declines in SCA and SWE reveal three distinct melt phases characterized by 1) low melt rates across a large area resulting in a minor change in SCA, but a very large decline in SWE with, 2) high melt

rates resulting in drastic declines in both SCA and SWE, and 3) low melt rates over a

small portion of the basin, resulting in little change to either SCA or SWE. The ability to

capture high-resolution spatio-temporal changes to tundra snow cover furthers our

understanding of the relative importance of various land cover types on the snowmelt

timing and amount of runoff available to the hydrological system during the spring

freshet.

Introduction

Snow cover is a keystone feature of Arctic landscapes, with the snow covered period being up to eight months in duration and end-of-winter snow cover accounting for up to 80% of the annual precipitation (Prowse and Ommanney, 1990; Yang et al., 2005; Young et al., 2006). This long snow covered period has significant effects at the local, regional, and global scale, including effects on: climate, surface energy flux, water balance, permafrost, vegetation, and terrestrial and aquatic ecosystems (Lantz et al., 2013; Marks and Dozier, 1992; McFadden et al., 2001; Rees et al., 2014). Although snow is clearly important to the Arctic environment, our ability to measure, and predict, key aspects of the snow environment are extremely limited and prone to very high errors sourced from measurement techniques and an inability to capture spatial heterogeneity across multiple scales.

During the winter accumulation period, our ability to quantify the snow environment is greatly challenged by the following. First, measuring snowfall is prone to very large errors due primarily to the effects of wind speed, with snowfall typically underestimated by 10 to 120% across the Arctic (Goodison et al., 1998; Pan et al., 2016; Yang et al., 2005). Ongoing research is attempting to solve this problem, but with limited success to date (Macdonald and Pomeroy, 2007; Sevruk et al., 2009; Thériault et al., 2012). Secondly, blowing snow results in an estimated sublimation rate of 20% to 40% of winter snowfall (Pomeroy et al., 1999, 1997; Pomeroy and Gray, 1995; Sexstone et al., 2016), but current estimates have extremely large uncertainties as winter measurements are prone to large errors. Eddy covariance methods may measure sublimation over the entire winter, however technical restraints restrict the

availability of data and therefore result in limited data. Finally, blowing snow erosion, transportation, and deposition results in a spatially heterogeneous snow cover (Pomeroy et al., 1997) with snow depths varying from a few centimeters on vegetation sparse uplands to many metres in snow drifts located in stream channels, lake edges, steep slopes and in tall vegetation patches. Developing sampling designs to measure this spatially heterogenous snowcover is challenging as standard terrain-based snow surveys that measure snow depth, density and water equivalent (SWE) across a watershed is extremely difficult and ensuring that snow drifts are accurately represented has proven difficult. Because of these data measurement limitations, it is currently not possible to balance winter snowfall, sublimation, and end-of-winter basin SWE with the precision necessary for understanding the snow cover and its various implications to other aspects of the environment. This results in significant limitations in understanding the effects of snow on all aspects of the environment and limits the ability to develop, test and use snow accumulation models. This problem is further exacerbated during the spring melt period when over snow travel is very challenging and conducting traditional snow surveys across broad areas is nearly impossible, therefore making it extremely difficult to document the changes in SWE over the melt period. Recent studies have attempted to address this through high resolution monitoring of the snow cover through the NASA Airborne Snow Observatory (ASO) in the Californian Sierra Nevada Mountain range, with great success (Painter et al., 2016; Raleigh and Small, 2017). However, to the Authors knowledge few if any studies have carried out such an analysis in the Arctic. This is a significant limitation to both understanding and modelling changes in snowcover over the melt period and resulting streamflow.

The spatially variable Arctic snowcover also has significant implications on snowmelt runoff as large snow drifts contain a large percentage of water relative to the surrounding landscape and add a layer of hydrological complexity to the snowmelt period (Marsh et al., 2008). These drifts will remain weeks to months after all snow is removed from non-drift locations and provide streams with ample melt water late into the spring, or early summer, resulting in high flows rates long after the initial freshet peak (Marsh and Woo, 1981; Quinton et al., 2004; Quinton and Marsh, 1998a). An inability to measure changes in SWE across watersheds during the melt period greatly limits our understanding of the processes controlling streamflow during melt, and also limits our ability to develop and test the required high-resolution physically based distributed models (Clark et al., 2011; Marsh et al., 2018; Peters-Lidard et al., 2017; Pomeroy et al., 2007; Sivapalan, 2018). In order to develop, test and apply such models, there is an urgent need for greatly improved snow data sets in Arctic regions.

Recent advances in Unmanned Aerial Systems (UAS) and *Structure-from-Motion* (SfM) photogrammetry methods allow the development of high resolution mosaics and digital surface elevation models, with accuracies comparable to traditional surveying techniques (Colomina and Molina, 2014). Recent studies have applied *SfM* photogrammetry to map snow depths across small open areas (Bühler et al., 2016; De Michele et al., 2016; Harder et al., 2016; Vander Jagt et al., 2015). These studies demonstrate the effective application of UAS and SfM for quantifying snow depths at sub-meter scales, with errors ranging from 8 to 30 cm relative to observed in-situ snow depth measurements. Mann (2018) demonstrated that these methods are sufficiently advanced to map end-of-winter SWE across an Arctic watershed, but to the authors

knowledge, this method has not been used to quantify declines in water storage and snowmelt patterns across the spring snowmelt in headwater tundra environments. As a result, there is an urgent need to test and apply UAS SfM methods to better understand the snowmelt period, and to provide the data sets required for predictive model testing.

Given these significant deficiencies in our ability measure spatial and temporal changes in snow over the melt period, the objectives of this paper are to test UAS methods to map micro-scale (1 meter resolution) SCA, snow depth and SWE on a daily time scale across the snowmelt period. This will allow for the documentation of observed changes in snowcover at previously unobtainable spatio-temporal resolutions as needed for improved understanding of snowmelt patterns and spring freshet timing and magnitude. A further analysis of changes in SCA and SWE for four major landcover types reveals important insights into spatio-temporal changes in snowmelt patterns at a basin scale. A further objective of this paper is to demonstrate how UAS mapping methods can be applied operationally across the Arctic as needed to better document spatial variability of snow cover as urgently required to address many water resource issues.

Study site

This study focuses on the Siksik Creek (68.74N, -133.49W) research watershed (Figure 2.1) that lies in the southern Tuktoyaktuk Coastal Plains and east of the Mackenzie Delta. The 95-hectare basin drains south into Trail Valley Creek (TVC), which then flows into the Arctic Ocean through the Eskimo Lakes (local name is Husky Lakes) estuary network. The Siksik basin, situated 50 kilometers north of the Inuvik Airport and 75 km south of Tuktoyaktuk on the Beaufort Sea coast, is underlain by

continuous permafrost extending between 150-350 meters below the surface (Heginbottom and Radburn, 1992), with active-layer depths range from 30 to 120 centimeters. Characteristics of the Siksik Creek catchment are biophysically similar to those of the larger Trail Valley Creek basin (Marsh et al., 2010), however, unlike the surrounding region the Siksik Creek catchment is free of lakes.

Siksik vegetation is typical shrub-tundra consisting of mosses, lichen, grasses and low-lying shrubs (*Betula*), patchy tall shrubs (*Alnus* and *Salix*), and spruce forest patches (Marsh and Pomeroy, 1996). As tundra snowcover is strongly influenced by vegetation, Marsh and Pomeroy (1996) and Pohl and Marsh (2006) mapped vegetation and hillslopes in TVC (including Siksik) for the purpose of mapping snowcover by landscape type. Marsh and Pomeroy (1996) classified landcover as tundra, tall shrub, and forest, while Pohl and Marsh (2006) used lidar to map vegetation height. However, shrubs across the study area are known to be changing rapidly (Lantz et al., 2013) and as a result, there was a need to update these earlier landcover maps. This revised landcover map was developed using a combination of methods. A supervised image classification was used in *ArcGIS* software using high-resolution UAS imagery collected in the fall of 2016 before leaf-off was used to map vegetation type. As snow drifts commonly form on steep slopes, we followed the methods of (Marsh and Pomeroy, 1996; Pomeroy et al., 1997) and classified slopes with gradients greater than 9°. We confirmed that these slopes develop snow drifts by comparing the location of 9° slopes to the location of late lying snow drifts as mapped from UAS images on 21 May, 2016. The resulting land cover classification is shown in Figure 2-2. Tundra, which covers 54% of the total catchment area, features relatively flat terrain with a rough micro-

topography consisting of mineral earth hummocks (Quinton and Marsh, 1998b). The predominant tundra vegetation includes lichen, moss, herbs and other patchy dwarf shrubs rarely exceeding 0.2 meters in height (Figure 2-3a). Short shrubs cover 28% of the watershed and are characterized by dwarf birch shrubs (*Betula nana*) that typically range in height from 0.2 to 1 meter (Figure 2-3b). Tall shrub patches cover 13% of the landscape and includes both green alders (*Aluns viridis*) and arctic willows (*Salix arctica*). Green alders in these patches are up to 3 m in height and occur in small patches that are scattered across the landscape and are predominantly located on the larger hillslope regions (Figure 2-3c), Willows in this zone occur primarily in the Siksik Creek riparian zone. Topographic drifts (Figure 2-3d) cover 6% of the watershed and occur where a break in slope results in windblown deposits of snow accumulating over the winter months. For the Siksik Creek basin these features are predominantly located along east and north-eastern facing slopes. Field observations demonstrate, as observed across Trial Valley Creek (Pomeroy et al., 1997), that drifts reoccur annually in the same locations, although the size of the drift varies from year to year. It is important to note that these topographic controlled drifts are defined by topography, and that there is a significant overlap with tall shrubs. Nearly 90 percent of the topographic drifts in this study area are underlain by tall shrub vegetation. The topographic drift land cover type is not considered mutually exclusive from the remaining hydrological landscape units defined by vegetation type.

The climate of this region is characterized by short, cool summers and long, cold winters. Much of the annual precipitation falls between late August and October with rain dominating the August-September months and snow in October, with over half of

the annual precipitation falling as snow (Mann, 2018). The end-of-winter snowcover

varies spatially, with substantial amounts of snow stored in large hillslope and channel

drifts. The onset of the spring snowmelt at Siksik typically begins in May when

temperature increases above 0°C (Pohl et al., 2006). Snowmelt rates are high, and the

snow covered area can decrease rapidly over a short period of 1-2 weeks (Pohl and

Marsh, 2006). This rapid removal of the snowcover, in combination with the shallow

active layer (Quinton and Marsh, 1999) results in the spring freshet which dominates the

annual hydrograph, with nearly 90 percent of the annual discharge occurs during this

short spring freshet period (Marsh et al., 1995), after which streamflow is controlled by

rainfall. These drifts contribute large portions of meltwater runoff late into the spring

season (Quinton and Marsh, 1998a).
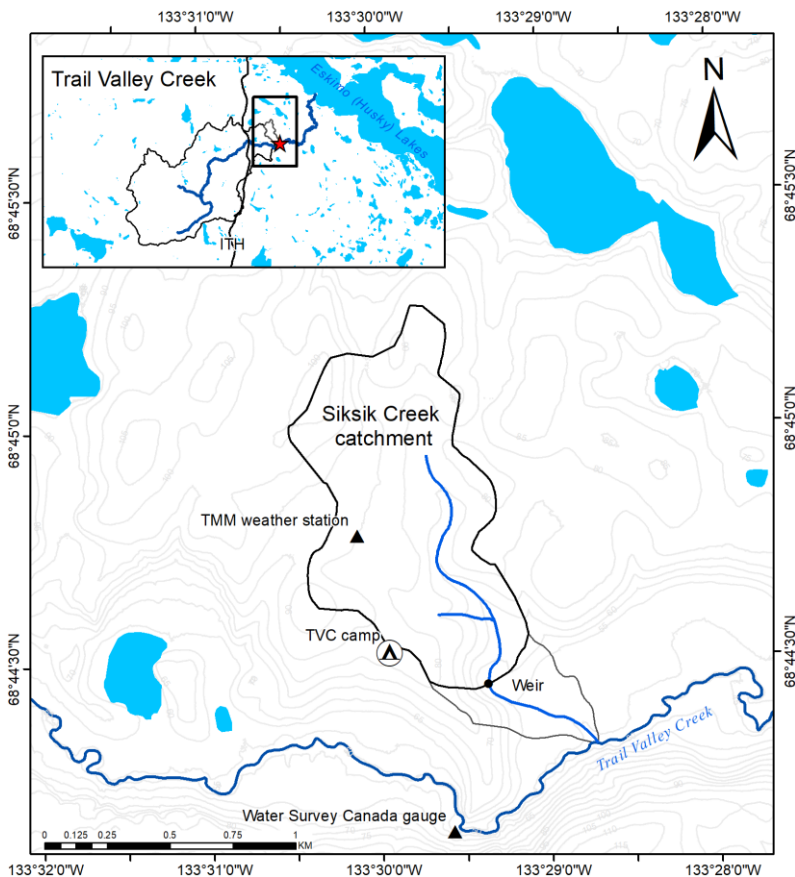
Figure 2-1: Location and topography of the Siksik Creek catchment located in the Trail Valley Creek watershed located 50 km north of the Inuvik, NWT airport. The drainage area upstream of the weir is 82.8 hectares. The total basin area is 95 hectares.
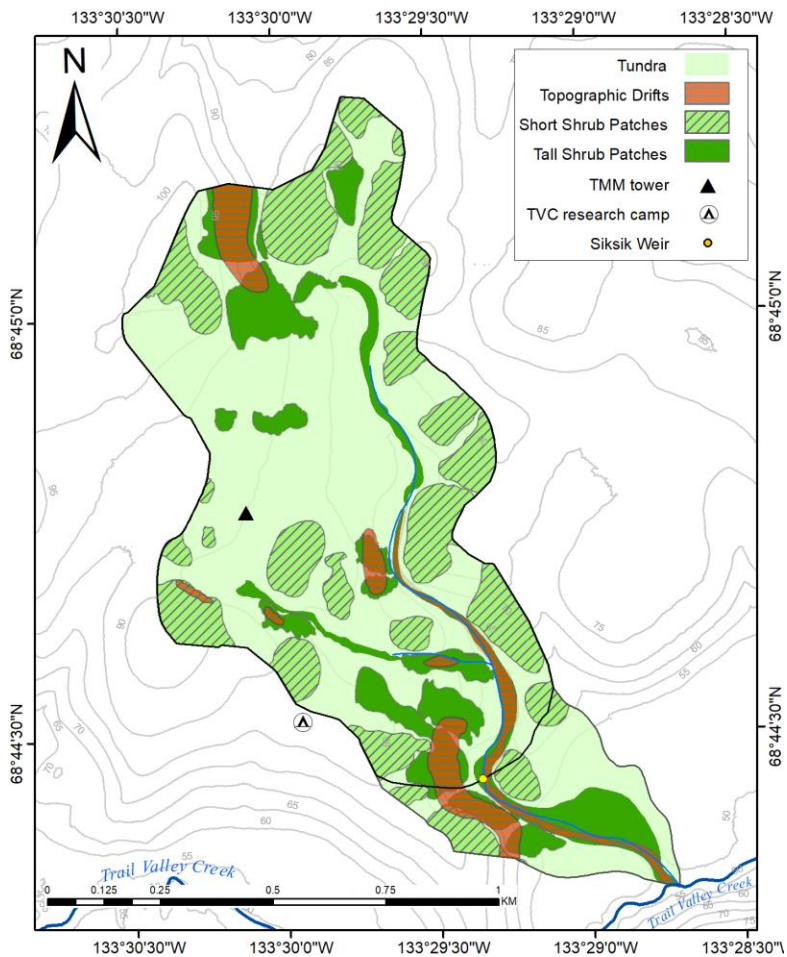
Figure 2-2: Siksik Creek catchment showing predominant land cover types. The majority of the basin is classified as open tundra with low lying vegetation. Short shrub patches consist primarily of dense dwarf birch while tall shrub patches feature a combination of green alder and tall willow shrubs. Drift features are defined by topography and the presence of late-lying snow drifts.
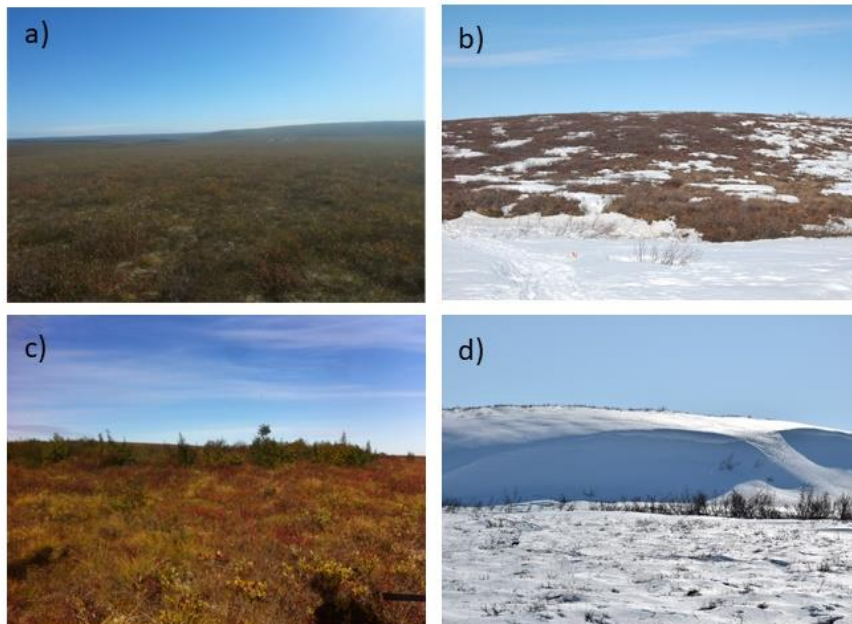
Figure 2-3: Primary land cover types characteristic of the Siksik Creek basin. Photographs show a) tundra, b) short shrubs early in the melt, c) tall shrub patch, and d) topographic drift sites.

Methodology

High resolution mapping of snow depth, area and water equivalent using UAS

High resolution Unmanned Aerial Systems (UAS) images of the snow covered Siksik basin allow for the production of digital orthorectified mosaics (orthomosaic) and Digital Surface Models (DSM). The DSM provides an accurate estimation of the snow surface elevation, from which a bareground Digital Elevation Model (DEM) is subtracted to reveal the snow depth, estimated as the difference between the two elevation datasets. Nolan *et al.* (2015) demonstrated the use of manned aircraft to obtain airborne photography and the use of *Structure-from-Motion* (SfM) technique to successfully map snow depths using georeferenced aerial imagery with high precision and accuracy. The application of affordable UAS technology over the last few years has for the first time enabled hydrologists to create high-resolution snow covered area and snow depth products at catchment scales with efficiency and accuracy at greatly reduced costs compared to other snow depth remote sensing methods. Recent studies by Bühler *et al.*, (2017), Harder *et al.*, (2016) and Wainwright *et al.*, (2017) for example, have demonstrated the success of this methodology for mapping snow depth and snow covered area, however none to date have focussed on continuing observations over the melt period which represents a challenge for both hydrologist and remote sensors.

This study utilized the *SenseFly EBEE UAV Ag* carrying an integrated onboard Sony S110 12 megapixel RGB camera with a 4000x3000 pixel resolution. Further UAS details are in (Appendix 2). The UAV flight plan was programmed using *eMotion 2* software, with the flights flown at 100 meters Above the Take-off Altitude (ATO) in a series of transects perpendicular to the predominant wind direction. To cover the entire

study basin, including a large boundary around the basin perimeter, multiple flights were flown back to back to cover the desired study area at a 2.8-centimeter ground sampling distance (GSD). Twelve ground-control points (GCP) were installed in April across Siksik Creek and georeferenced using a *Leica Global Navigation Satellite System (GNSS) Real-Time Kinematic GPS* system with a 3-dimensional accuracy of ±<0.02 meters. GCPs increased the accuracy of the DSMs, specifically for the Z axis (elevation) which is the most important for measuring snow depths (Appendix 3). Although we planned daily data acquisition over the duration of the 2016 spring (April-May) period for the entire Siksik Creek catchment, actual data acquisition was limited by weather conditions. The complete dataset used in this paper consisted of 14 flights across 29 days between 23 April and 21 May 2016. The area encompassed by each series of flights for each date was 2.5 km^2 ensuring ample coverage of the area surrounding the <1 km^2 catchment boundary.

Photographs from each UAS flight were processed using the photogrammetry software *Pix4D* resulting in the creation of a high-resolution Orthomosaic consisting of red, green, and blue wavelengths and a Digital Surface Model (DSM). Despite a snow cover that has a high albedo and limited surface features, sufficient snow surface features were present for the SfM photogrammetry software to distinguish common tie points across the imagery and produced desired mosaic and DSM outputs. GCPs were input during the processing stage to produce DSMs with estimated vertical accuracies ranging from 0.02-0.10 m elevation. Without GCPs the standard elevation error was around ± 2-5 meters resulting from errors in the standard onboard GPS receiver equipped on the UAV.

A GIS model (Figure 2-4) was created to automate the quantification of snow covered area, snow depth, and snow water equivalent. This model incorporates the UAS orthomosaic and DSM for each flight, requiring only user inputs of snowpack density to estimate SWE. Methods for measuring snow density are provided below. The resulting UAS products were then analysed further and classified into four landscape hydrological units representative of the basin based on dominant vegetation and topography as outlined in the study site section.

Snow depth mapping:

Snow depth maps were created for each UAS flight during the 2016 spring melt period, resulting in 14 successful snow depth products for Siksik Creek. Snow depth was calculated for each pixel within the study area by subtracting two high-resolution raster layers from one another (Equation 1). Snow depth, as estimated the GIS model (Figure 2-4), subtracts a snow-free raster dataset from the snow-surface DSM obtained with the UAS. This study applied a bareground lidar product produced in 2008 for the entire Trail Valley Creek domain (Hopkinson et al., 2008) as we believe that it provides a better estimate of the surface elevation with a reported 0.13 m vertical accuracy and required no corrections for vegetation, unlike the UAS bareground DSM collected in the fall season. The bareground lidar applied in this study features a spatial resolution of 1 m, and therefore required the UAS product to be upscaled to 1 m resolution. UAS resolution was rescaled during the processing stage using *Structure-from-Motion* software. Snow depth for each raster cell is then calculated as:

$$h_x = DSM_{snowx} - DEM_{ground} \qquad\qquad (1)$$

Where: h_x is snow depth for each pixel cell, x is the date of UAV flight, DSM_{snow} is the snow surface elevation from the UAV and DEM_{ground} is the elevation of the bare ground with no vegetation

A snow-free area mask was incorporated into the model in order to avoid any errors related to apparent changes in surface elevation due to the emergence of previously buried shrubs causing false surface elevation measurements in snow free areas. Snow surveys were conducted across representative land units within the Siksik Creek catchment to provide ground validation data for the UAS snow depth products and to provide snow density measurements. These surveys were repeated at multiple transects representing the variations in land cover type to capture the spatial distribution of the snow depths across the catchment. Snow depths were measured using a GPS Magnaprobe snow depth measuring device (SnowHydro, 2013a; Sturm et al., 1999) consisting of a metal probing rod and sliding basket that relays the snow depth along with the corresponding GPS position to a Campbell Scientific datalogger. The Magnaprobe GNSS receiver features a 5-10 m absolute horizontal GPS accuracy. Snow depth measurements were collected at 1 m intervals along 25-100 m transects as shown in (Figure 2-5). Measurements of SWE in shallow snowpacks were obtained using a clear Lexan ESC-30 snow corer (SnowHydro, 2013b) with cutting teeth for depths under 1.2 m every 5- 10 m. For snowpacks exceeding the depth of the snow corer tube, such as those observed in large snow drifts, a Standard Federal snow sampler corer (Goodison et al., 1987) was used. The snow samples obtained via the snow corer are weighted and depths recorded to provide the snowpack density and SWE at a given point. Previous comparison of snow corers by Dixon and Boon, (2012)

demonstrated the two snow corers applied in this study show similar SWE error

estimates. A summary of UAS flights and corresponding in-situ measurements of

magnaprobe snow depth and SWE snow surveys is summarized in Appendix 4.

Snow covered area:

Snow covered area (SCA) was quantified at high resolution (0.1 m GSD) using

the UAS output orthomosaic and image classification software included in the *ArcGIS*

software. A binary image classification was produced distinguishing between snow-

covered and snow-free areas using an unsupervised image classification conducted for

each flight using the ISO Clustering method from the *Image Analysis* package. In the

case that this technique could not accurately distinguish between snow-covered and

snow-free areas (often resulting from shadows on steep topographic features, dirty
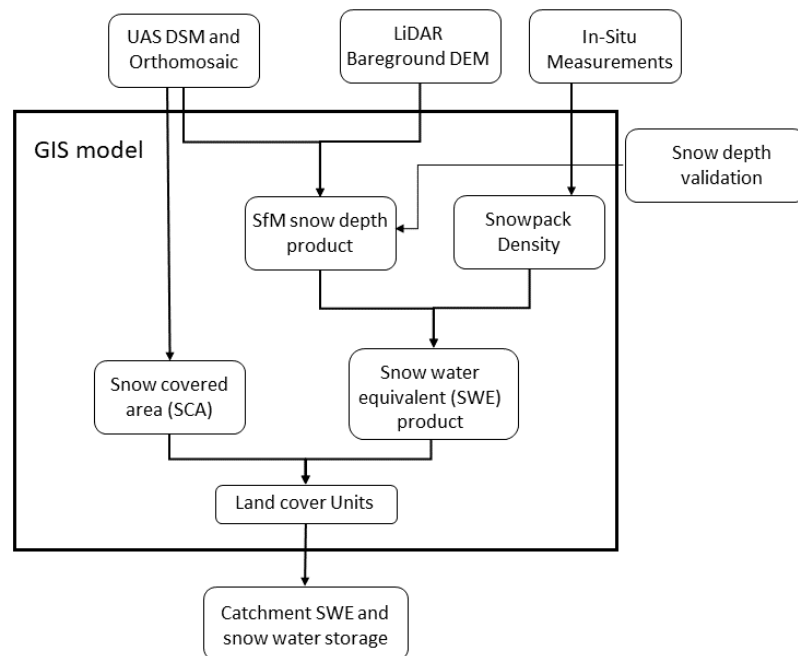
Figure 2-4: A conceptual model of the inputs and methods applied to measure snow depth, snow covered area, SWE, and water storage within the Siksik Creek catchment using the Structure-from-motion UAS imagery. A GIS model was created resembling this conceptual model.

snow surfaces resulting from blowing road dust or vegetation protruding above snow) a

Maximum Likelihood supervised classification was employed by using output specific

training sites created by the user. SCA was documented as aerial coverage (m^2) and

converted to a percentage of the basin area.
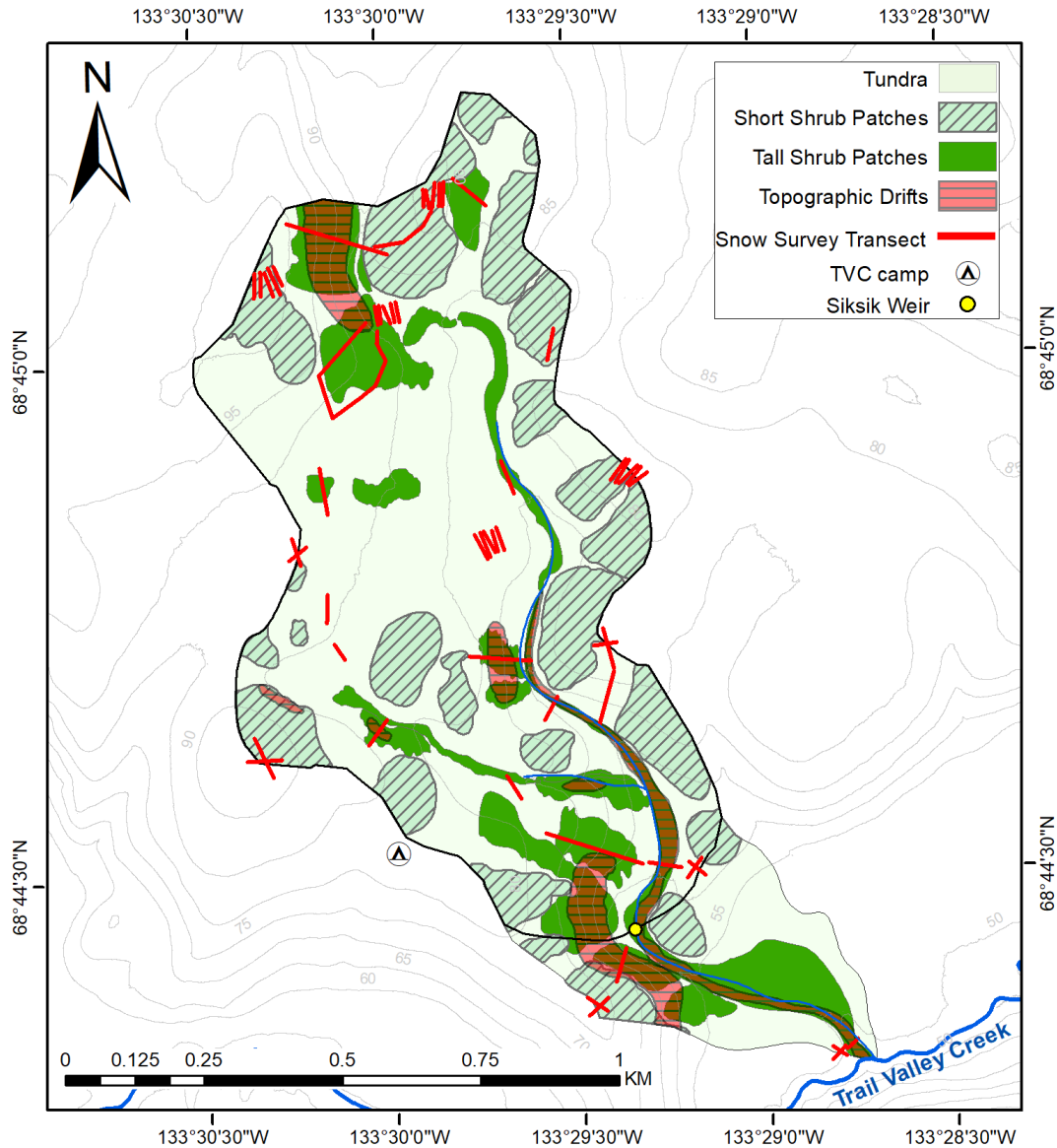
Figure 2-5: Location of Siksik Creek repeated snow survey transects for the 2015-16 season (red lines). Snow depths were collected at 1-meter intervals using a GPS magnaprobe instrument. Snow core measurements were taken every 10 snow depths using an ESC-30 style snow corer. A Standard Federal sampler was used for snow depths greater than 160 cm.

<u>Snow water equivalent:</u>

Previous studies have typically estimated basin average SWE from terrain based snow surveys of snow depth and density weighted by terrain area (Marsh et al., 2008). Using UAS based methods to map snow depth provides the possibility of mapping SWE as well. However, to do this requires estimates of snow density at the same resolution for all points across the watershed. Previous studies using UAS or lidar based methods to measure snow depth have estimated density from relationships between snow depth and density (Mann, 2018; Raleigh and Small, 2017) or from physically-based (Marks and Dozier, 1992) or empirical density models (Sturm et al., 2010). Both methods have significant errors and introduce limitations and uncertainties in final SWE products.

In this study, estimated snowpack densities from snow depth-density linear regression equations between measured in-situ snow depth and density observations collected across the catchment at various sites using the survey methods noted above. Snow survey data collected across various representative landscape types were averaged on a site basis to produce depth-density relationships for each survey date (Figure 2-6) over the full snowmelt period. For example, if 20 snow corer measurements were obtained across a single snow survey transect these values would be averaged and serve as one point on the depth-density plot for said given date, with each depth-density curve consisting of multiple snow survey sites (n=20 to n=4). An overview of the average survey depth, density, number of snow survey transects, and linear regression equations are displayed in Table 1. This method for estimating snow density was incorporated into the model (Figure 2-4) as it was deemed the most efficient approach to account for greater snow density with increasing snow depth, while also considering

snowpack density which includes increased liquid water content over duration of the

snowmelt (Marsh 1987; Marsh and Woo 1984). To apply such UAS methods across the

Arctic will require much improved methods to model or estimate snow density.
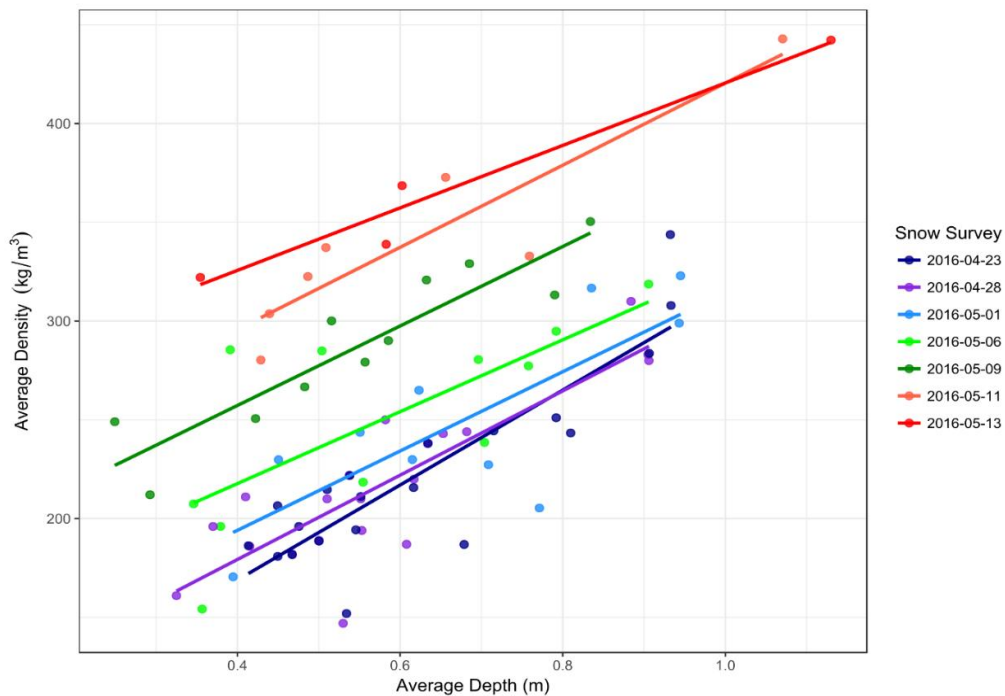
Figure 2-6: Snow depth-density linear regression relationships used for incorporating spatial variability of density to calculate snow water equivalent in the GIS model. Colours show data points collected by date. Average snow density, shown on the Y axis, gradually increased over time due to the increasing liquid water contained in the snowpack pore space.

Estimation of melt rates:

Temporal changes in basin SWE (ΔSWE) over the melt period are quantified as

the decline in UAS derived SWE between two consecutive dates for basin average

SWE. Missing data for dates between UAS acquisitions were gap filled via linear

interpolation between consecutive observations. With both SCA and SWE mapped

across the watershed, it is then possible to determine changes in basin SCA and

average SWE. From these, it is for the first time possible to determine basin average

melt rate from observations, rather than estimating via snowmelt models. Given the

current errors in measuring snow depth from UAS and estimating snow density, it is

likely that the errors are too large to estimate small melt rates at a single point across

the watershed, but are likely sufficient to estimate average basin-wide snowmelt rates

as follows:

$$M = \frac{(\Delta SWE)}{(SCA_1 + SCA_2)/2} /100 \qquad (2)$$

Where *M* is basin average snow melt rate per unit snow covered area (mm/day),

ΔSWE is the decline in basin average SWE, and *SCA₁* and *SCA₂* are the basin

watershed snow at time 1 and time 2.

Table 1: Summary table of average snow depth and density measurements for Siksik catchment over the duration of the 2016 melt obtained from in-situ snow surveys. Each snow survey consists of 5-20 individual measurements of snowpack depth and density obtained using a snow corer. Snow surveys were repeated along the same transects over the melt period. Depth-density linear functions were created for each date and are summarized in the final two columns. Linear equations for SWE were applied to each snow depth pixel for a corresponding UAS SfM product.

Survey Date	Average Depth (m)	Average density (Kg/m^3)	No. of snow survey sites	Equation for SWE	R^2
April 22, 2016	0.62	222	20	= ((240.31*(x) + 72.8)*(x))	0.76
April 28, 2016	0.58	218	20	= ((210*(x) + 94)*(x))	0.72
May 1, 2016	0.68	251	10	= ((200*(x) + 113.8)*(x))	0.60
May 6, 2016	0.58	251	11	= ((180*(x) +144.9)*(x))	0.51
May 9, 2016	0.55	287	11	= ((200*(x) + 176.8)*(x))	0.84
May 11, 2016	0.62	342	7	= ((210*(x) + 212.6)*(x))	0.77
May 13, 2016	0.67	368	4	= (160*(x) + 262.4)*(x))	0.95
May 17, 2016	0.29	500[1]	1	= x*500	NA

[1] Maximum density assumed for remaining deep snow drifts includes incresed liquid water content

<u>Validation of UAS snow depths:</u>

Point-to-point snow depth comparisons from snow survey depths and UAS (Figure 2-7) show wide variations between both methods. Such a weak agreement between Magnaprobe vs UAS snow depths was also found by Nolan *et al.* (2015) who suggested this weak agreement resulted from a co-registration error between the high spatial accuracy of SfM derived snow depth product and the low spatial accuracy Magnaprobe measured snow depths. Small-scale heterogeneity of snow depths is known to vary significantly over very short distances as demonstrated by Mann (2018). Because of this point-to-point overlay of probe depths (low horizontal GPS accuracy) results in moderate correlation coefficients (r ranging from 0.72 to 0.49) and relatively high root mean square errors (RMSE range from 0.21 m to 0.54 m with an average of 0.34 m) when compared to the highly accurate DSM outputs from the UAS-derived snow depth raster values. Statistics for each comparable date are presented in the text insets of Figure 2-7.

Another method to validate the UAS SfM snow depth maps is to consider the statistical similarities between the observed and UAS snow depths across all available data. Figure 2-8 and Table 2 show the summary statistics and probability density functions (PDF) for all snow depths collected using the UAS and in-situ measurements. To compare the distributions a two sample Kolmogorov-Smirnov test for each PDF distribution was undertaken revealing a strong likelihood that the two methods represent snow depth distributions from a similar distribution at the 95% confidence interval. Kolmogorov-Smirnov critical values are presented in the text insets of Figure 2-8.

Across the study period similar mean snow depth, standard deviation, and coefficient of variation are observed for all available dates revealing near identical values, however the sample sizes differ by several orders of magnitude, and the snow survey method can not fully sample the full range of shallow and deep snow depths. For example, on 23 April 2016 1339 manual snow depth measurements were collected across the basin based on the snow survey transects while the UAS SfM estimated snow depth for ~950,000 points. The UAS SfM product does present a positive bias when compared to observed depths (absolute biases range from 0.17 m to 0.32 m), however uncertainties and sampling errors associated with snow depth observations make it difficult to conclude whether manual depth measurements accurately represent the spatial distribution of snow depths across the basin. Previous work by Berezovskaya and Kane (2007) found a tendency for manual probe snow depth may be subject to overestimations of snow depth of approximately 11-31% in tundra environments due to over probing and penetration into the underlying vegetation and unfrozen soil. This represents a significant source of potential error for manually measuring snow depth in tundra environments and may explain some of the variation between observed and UAS snow depths. Unfortunately, the extent to which any potential over probing may influence the validation of UAS SfM snow depths is not known.

UAS SfM snow depth validation results presented in this study agree with those of previous studies (Mann 2018, Harder *et al.* 2016) and strongly suggest that UAS derived snow depth maps capture both the spatial distribution and basin average snow depths. Further advantages of using the UAS to map snow depth is that it provides complete coverage of the area of interest and allows mapping snow depths over a much

larger domains than a small team of snow surveyors can cover. This is especially important for mapping large watersheds and ensuring measurement of the full range of large drifts that are difficult to survey using traditional methods, and both hold a large percentage of total watershed SWE and play an important role in snowmelt runoff. The UASs ability to capture all the snow depths across a study area makes this method less subject to uncertainties associated with locations of snow survey sampling sites and spatial interpolations of snow depth as is common with traditional survey methods.

Technical errors from geolocation accuracies of the UAS SfM snow depth products is also a potential source of uncertainty, especially as the snow depth becomes shallow and snow depths fall within the measurement errors. A similar study by Harder *et al.* (2016) mapping snow depth with a similar fixed-wing UAV platform (Sensefly EBEE Plus RTK) found that mapping snow depths in shallow prairie snowpacks was hindered by the accuracy and precision of the UAS, citing difficulties mapping snow depths below 30 cm. Results of this study concur with that of Harder *et al.* (2016), and other SfM studies (Buhler et al., 2016; Bühler et al., 2017; Nolan et al., 2015; Vander Jagt et al., 2015).

Estimating Error:

Errors in snow water equivalent were estimated by multiplying the snow depth root-mean squared error (RMSE) (Figure 2-7 and Table 2) by an averaged daily snow density (Table 1) for each grid cell across the study area. The cumulative SWE for each grid cell was then normalized to the remaining snow covered area for each date to estimate a total basin SWE error as mm SWE. On average, estimated SWE error for any given grid cell ranged between 20-110 mm while basin average SWE error for the

entire Siksik Creek catchment ranged between 5-15% of the basin averaged SWE, with a positive bias compared to in-situ observations in both cases. Comparison of basin weighted average SWE estimated from manual snow surveys proved to greatly underestimate basin SWE resulting from the nature of the field sampling protocol featuring a primary focus of capturing the variations in snow depths rather than weighted SWE by land cover units. Estimates of UAS SWE error is heavily dependant on the quality of error estimates between in-situ snow depths and SfM derived snow depths. The relatively large SWE error is expected to have a more dramatic impact for shallow snowpacks as the snow depth in these regions falls within the effective accuracy of the SfM methodology as previously demonstrated by Harder et al., (2016).

Table 2: Snow depth summary statistics between In-situ GPS magnaprobe and UAS derived snow depths across comparable dates during the 2016 melt period. This table reveals similar descriptive statistics between the two methods and enables confidence in the final UAS snow depth maps. Important to notice is the slight degradation of statistical similarities towards the end of the melt due to an inability to accurately measure snow depth late into the snowmelt period using traditional methods due to restricted access to the remaining snowpacks. Bold r values are statistically significant at the 95% confidence interval.

Date		Number of samples	Average Depth (m)	St. Dev (m)	CV	Abs. Bias (m)	RMSE (m)	Pearson r Correlation
April 23, 2016	Probe	1,339	0.58	0.21	0.36	0.17	0.21	**0.65**
	UAS	960,550	0.57	0.27	0.47			
April 24, 2016	Probe	1,339	0.58	0.21	0.36	0.21	0.29	**0.63**
	UAS	956,363	0.69	0.31	0.45			
April 28, 2016	Probe	377	0.71	0.29	0.41	0.28	0.38	**0.59**
	UAS	926,765	0.66	0.31	0.47			
April 29, 2016	Probe	379	0.71	0.29	0.41	0.23	0.36	**0.64**
	UAS	918,718	0.62	0.27	0.44			
April 30, 2016	Probe	763	0.67	0.30	0.44	0.29	0.44	**0.58**
	UAS	943,423	0.66	0.34	0.52			
May 4, 2016	Probe	676	0.57	0.28	0.49	0.30	0.42	**0.43**
	UAS	900,099	0.52	0.52	1.00			
May 5, 2016	Probe	434	0.55	0.29	0.53	0.27	0.41	**0.66**
	UAS	894,986	0.47	0.33	0.70			
May 8, 2016	Probe	538	0.48	0.33	0.69	0.21	0.31	**0.71**
	UAS	797,720	0.29	0.27	0.93			
May 10, 2016	Probe	477	0.40	0.33	0.83	0.30	0.40	**0.54**
	UAS	688,214	0.34	0.34	1.00			
May 12, 2016	Probe	475	0.40	0.33	0.83	0.26	0.36	**0.58**
	UAS	240,281	0.22	0.32	1.45			
May 18, 2016	Probe	133	0.03	0.18	5.93	0.32	0.54	0.09
	UAS	23,834	0.32	0.42	1.34			
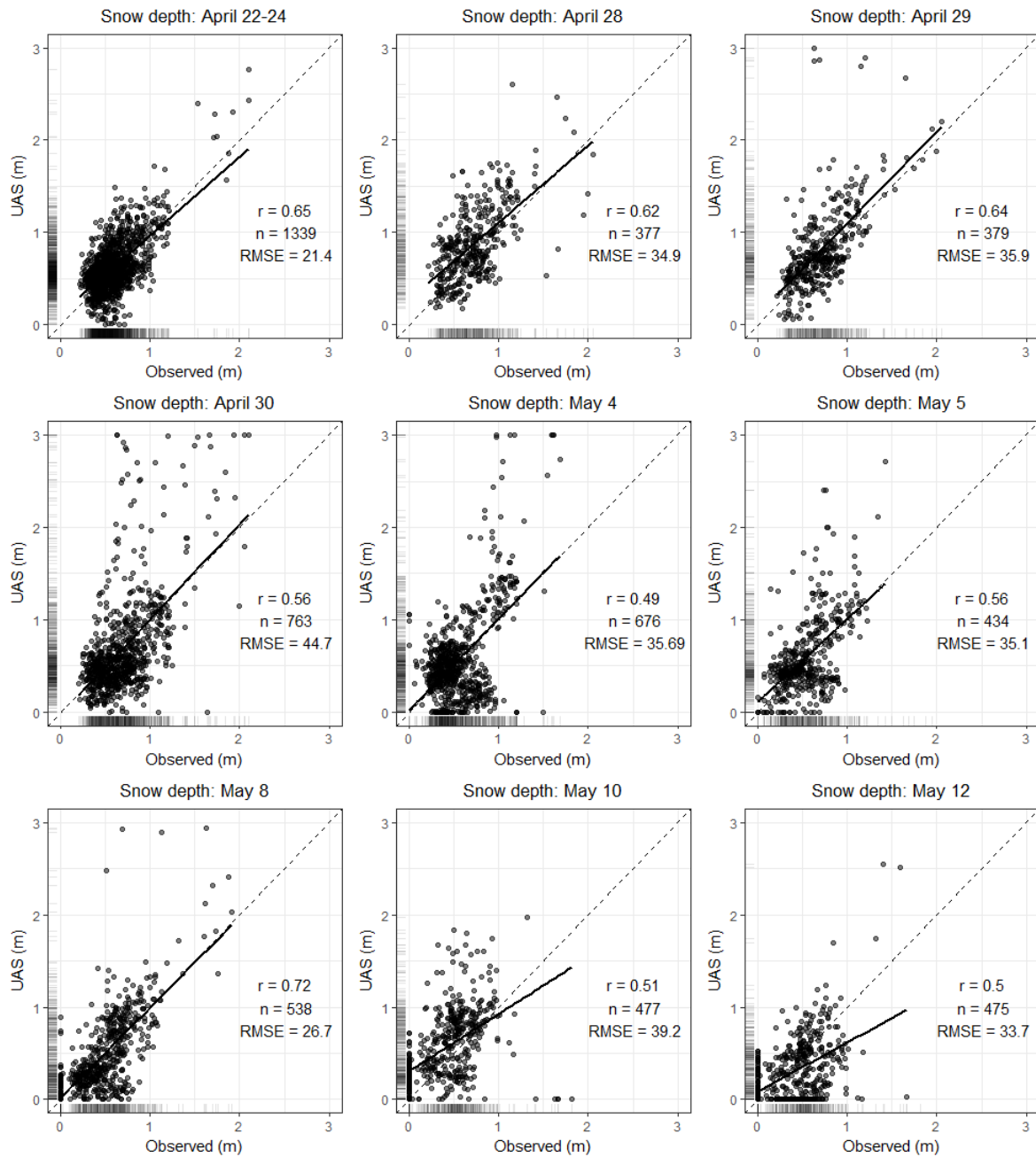
Figure 2-7: Scatterplot of UAS derived snow depths vs overlying in-situ observed snow depth using a Magnaprobe. Black lines show plotted line of best fit, grey dashed line shows 1:1 relationship showing perfect agreement between UAS and in-situ measurements. Rug plots on axis show density of points in the plotting area. A summary of correlation (r), sample size (n), and root mean square error (RMSE) is shown within each figure.
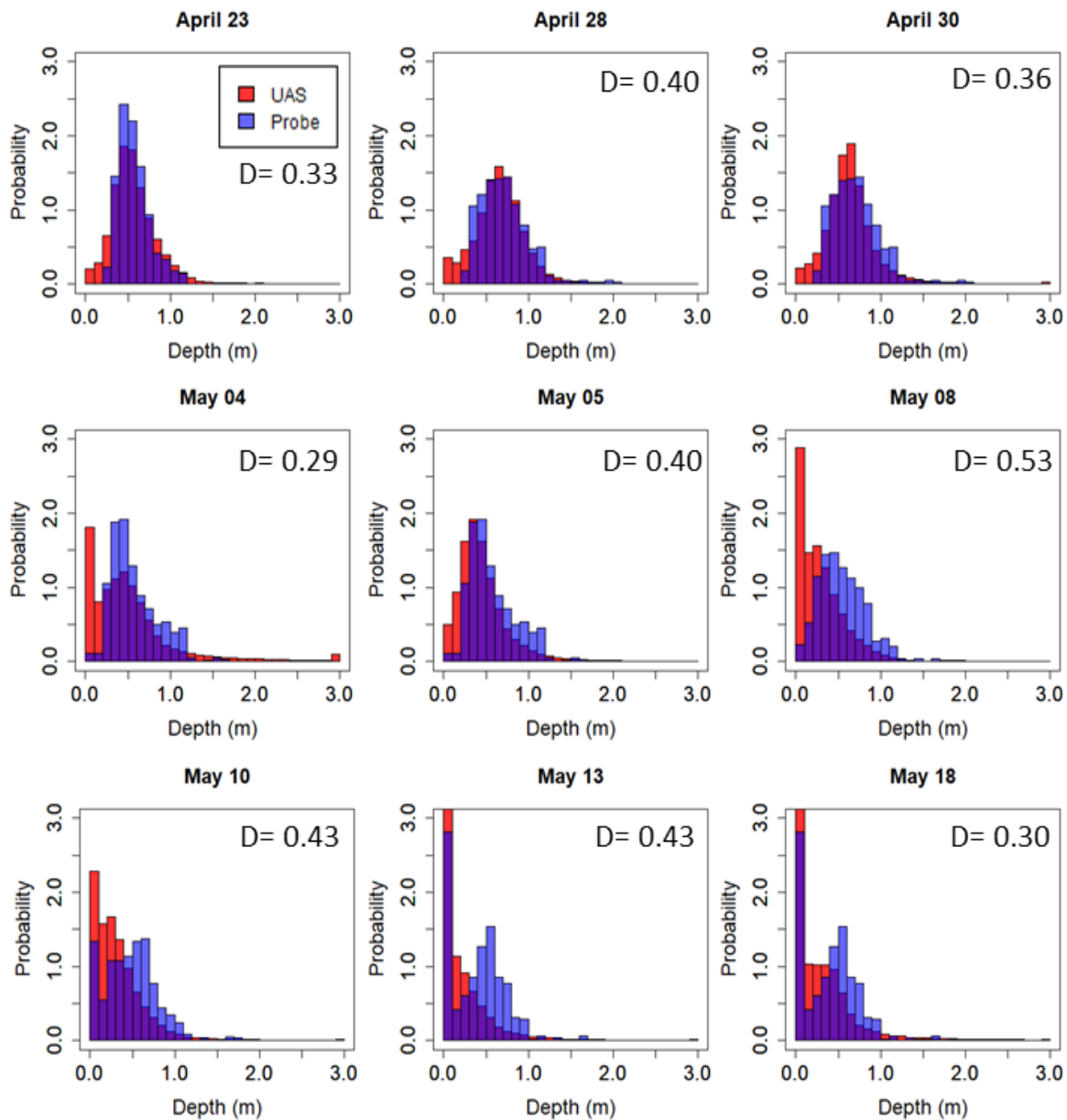
Figure 2-8: Probability distribution of all snow depths for UAS and Magnaprobe showing the probability of any random depth falling into a range of values. All snow depths from Magnaprobe (blue) and UAS SfM products (red) are included in the analysis. Purple reveals overlap in the PDFs. Similar PDF distributions demonstrate the strong likelihood that the two datasets are from the same population. Two-sample Kolmogorov-Smirnov test critical values (D) are presented in the top right.

Results

Previous studies (Busseau et al., 2017; Davison et al., 2006; Marsh et al., 2008; Pohl and Marsh, 2006) have addressed the spatial heterogeneity of tundra snowmelt, however they have been limited by a lack of appropriate high-resolution SWE data sets, and instead have relied on a combination of end-of-winter terrain based snow surveys and melt models to predict landscape changes in snow cover conditions. Here we address this deficiency that is typical of previous Arctic snowmelt studies through the UAS SfM platform, presenting for the first time high-resolution spatial and temporal data sets of micro-scale measurements of SCA and SWE over the duration of the spring melt.

Changes in watershed average snow covered area and water equivalent

At the onset of melt on 30 April basin SWE estimated by the UAS was 157 ±11 mm (Figure 2-9). This value is significantly higher than wind-corrected estimates of precipitation (Geonor; 88 mm) (Mann, 2018) and higher than end-of-winter SWE values estimated using weighted snow surveys (123 ±20 mm on 23 April 2016) (Mann, 2018). Mann (2018) attributed these differences to the well-known problems with snow gauge under catch and snow surveys under sampling deep snow drifts. Due to these reasons we conclude both methods provide an underestimation of snowfall and end-of-winter SWE accumulation. The following will focus on changes in SCA and SWE after the onset of melt (30 April).

Observed changes in basin SCA during melt, and the spatial pattern of such change, are shown in Figure 2-9, presenting similar patterns as described in previous studies, with the basin being mostly snow covered during the first phase of melt,

undergoing a slow decrease in SCA over this approximately one-week period. This is

followed by a second phase only a few days in duration that has an extremely rapid

decline in SCA, as the basin quickly transforms from completely snow covered to nearly

snow free. Figure 2-9 shows the deep snow drifts remain over this period and the areas

with shallower snow, as found across the majority of the study area, are rapidly

removed early in the spring melt period. Finally, entering the third phase only the deep

drifts remain on the landscape, and the SCA area is very low, with the watershed nearly

snow free. Phase 3 extends for a period of weeks as the snow from the deep drifts is

slowly removed from the landscape whereby some drifts remain until the end of June.

Unlike previous studies, the UAS based data allows for both spatial (Figure 2-9) and

temporal (Figure 2-10) analysis of observed changes in SWE over these three melt

phases across the entire catchment. The following sections provide details on these

combined changes in SCA and SWE and examines the three snowmelt phases:

Melt Phase 1: The initial melt phase (30 April to 08 May) is characterized by mean daily

air temperatures at or below 0°c (Figure 2-10a), daily average solar radiation below 100

W/m^2 (Figure 2-10b), and a small decline in SCA of 14% from 100% to 86% (Figure 2-

10c). The slow initial decline in SCA is similar to that described by numerous earlier

studies (Brown et al., 2010; Marsh et al., 2010; Marsh and Pomeroy, 1996; Wang et al.,

2005). However, despite the small decline in SCA over the 8 day period a 49% decline

in initial SWE was observed, from 157 mm to 80 mm respectively (Figure 2-10d).

Estimated SCA and SWE allow the estimation of snowmelt rates per unit area, across

the remaining snowpack, reveal an average melt rate of between 9.7 and 11.0 mm/day,

Phase 1
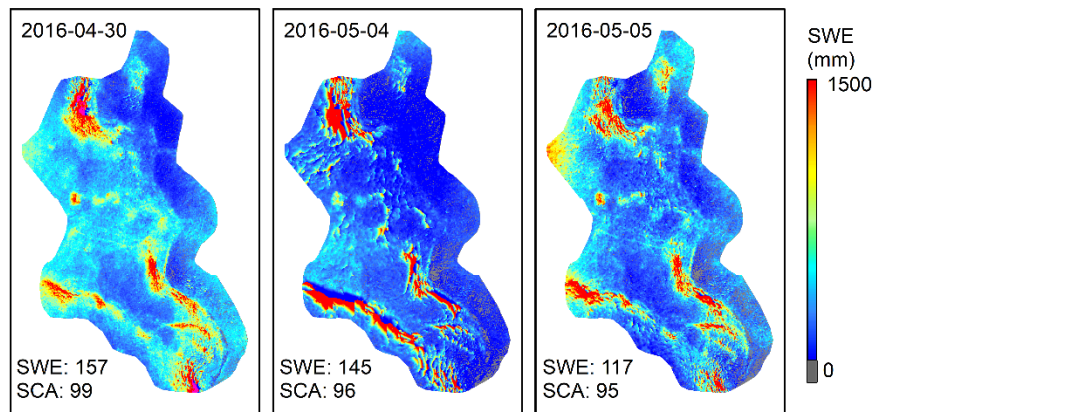
Phase 2
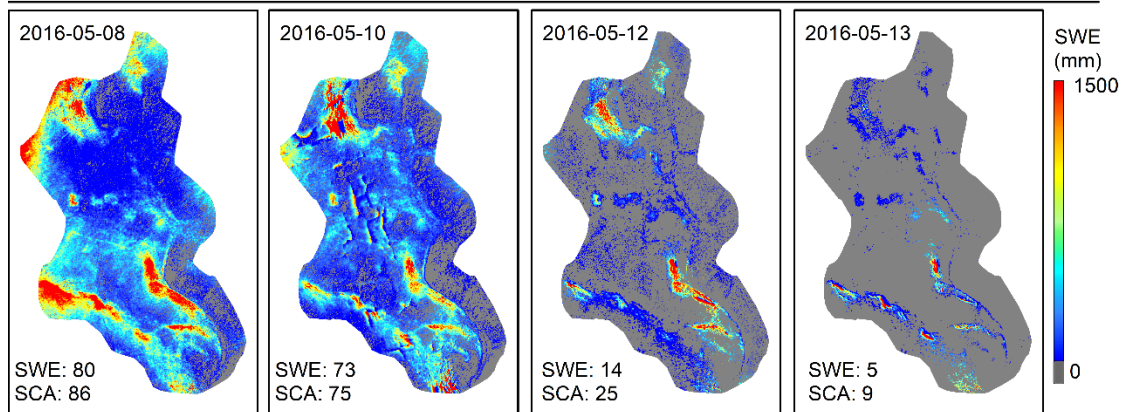
Phase 3
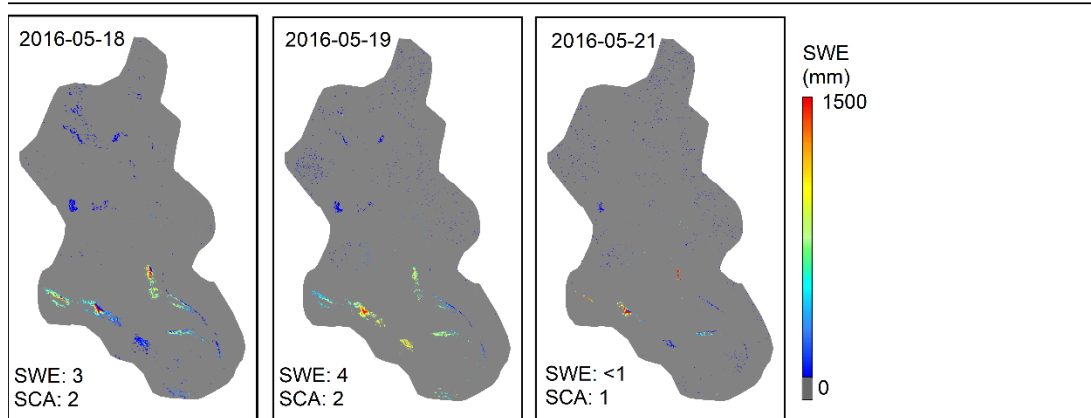
Figure 2-9: Snow water equivalent (SWE) maps produced using from the UAS for Siksik Creek.SWE (mm) and snow covered area (SCA) are presented in the bottom left corner for each date. Deep snowcover is shown in red with a high SWE, dark blue are areas with low SWE, while snow-free areas are shown in grey. Figures are sepreated by the three major melt phases described.

with an average of 10 mm per day (Figure 2-10e). The 2016 low melt rate during this phase was a result of low air temperatures and low shortwave radiation inputs. These estimated melt rates are similar to those observed previously by Marsh and Pomeroy (1996) who applied an energy balance model to suggest an average melt rate of approximately 10 mm/day during the first 10 days of the 1993 TVC melt period. In Phase 1 these low melt rates were distributed over the large snow covered area (over 95% of the watershed), resulting in the removal of almost half of the snow water equivalent, despite very little change in SCA. Such a large decline in SWE across the larger Trail Valley Creek during Phase 1 of the snowmelt was also suggested by Marsh et al. (2010). Although not directly comparable to the previous studies in this region by Marsh *et al.* (2010) and Marsh and Pomeroy (1996), we can conclude that the similar melt rates estimated by the UAS fall within the expected range during this phase of the melt.

Melt phase 2: The 5 day period from 08 May to 13 May, is characterized by unusually warm air temperatures that reached a maximum daily average of 14.5 °C (Figure 2-10a), with a peak of 20 °C at solar noon on 12 May, cloud free conditions with a maximum net shortwave radiation of 372 W/m^2 (Figure 2-10b), and strong southerly winds reaching peaks of 5 m/s. These conditions resulted in high melt rates, with the strong winds resulting in significant advection of sensible heat from snow free patches to the snow covered areas (Marsh et al., 1997). This resulted in a dramatic decrease in SCA from 86% to 9%, a 77% loss of SCA over the five day period. This rapid decline in SCA is similar to that described by Pohl et al. (2006) and others, is due to the removal

of snow from areas of the basin that featured a shallow end-of-winter snow cover, including short shrub and tundra regions.

Along with a drastic decline in SCA the second melt phase also features a large decline in basin SWE, with 75 mm of cumulative melt (47% initial SWE) occurring over the 5 day period. This phase also features large daily melt rates across the remaining snowpack rapidly increasing from 19 to 60 mm/day, with an average melt rate of 29 mm/day per unit snow covered area. Again, similar melt rates were estimated by Marsh and Pomeroy (1996) using an energy balance model to suggest an average melt rate of approximately 20 mm/day, rising to over 100 mm/day during Phase 2 of the 1993 TVC melt period.

During the warmest three day period (10-13 May), with very high temperatures and incoming shortwave radiation, the melt rate was up to 60 mm/day and removed 94% of the remaining SWE. ΔSWE, estimated as the basin difference in average SWE across consecutive dates over this three day period, accounts for 43% of the initial EOW basin SWE (ΔSWE of 68 mm) and also marked the largest decline in SCA (75% to 9%). Spatial data (Figure 2-9) from the UAS shows that on 13 May, the end of Phase 2, the only areas with snow were those that had end-of-winter deep snow drifts that formed from the deposition of blowing snow.

Melt phase 3: At the beginning of phase 3, when the SCA was only 9% of the basin area, daily average air temperatures cooled towards 0°c and solar radiation decreased, reducing the available energy contributing to melting the remaining snowpack. During this phase trace amounts of snow remain found in areas where blowing snow had
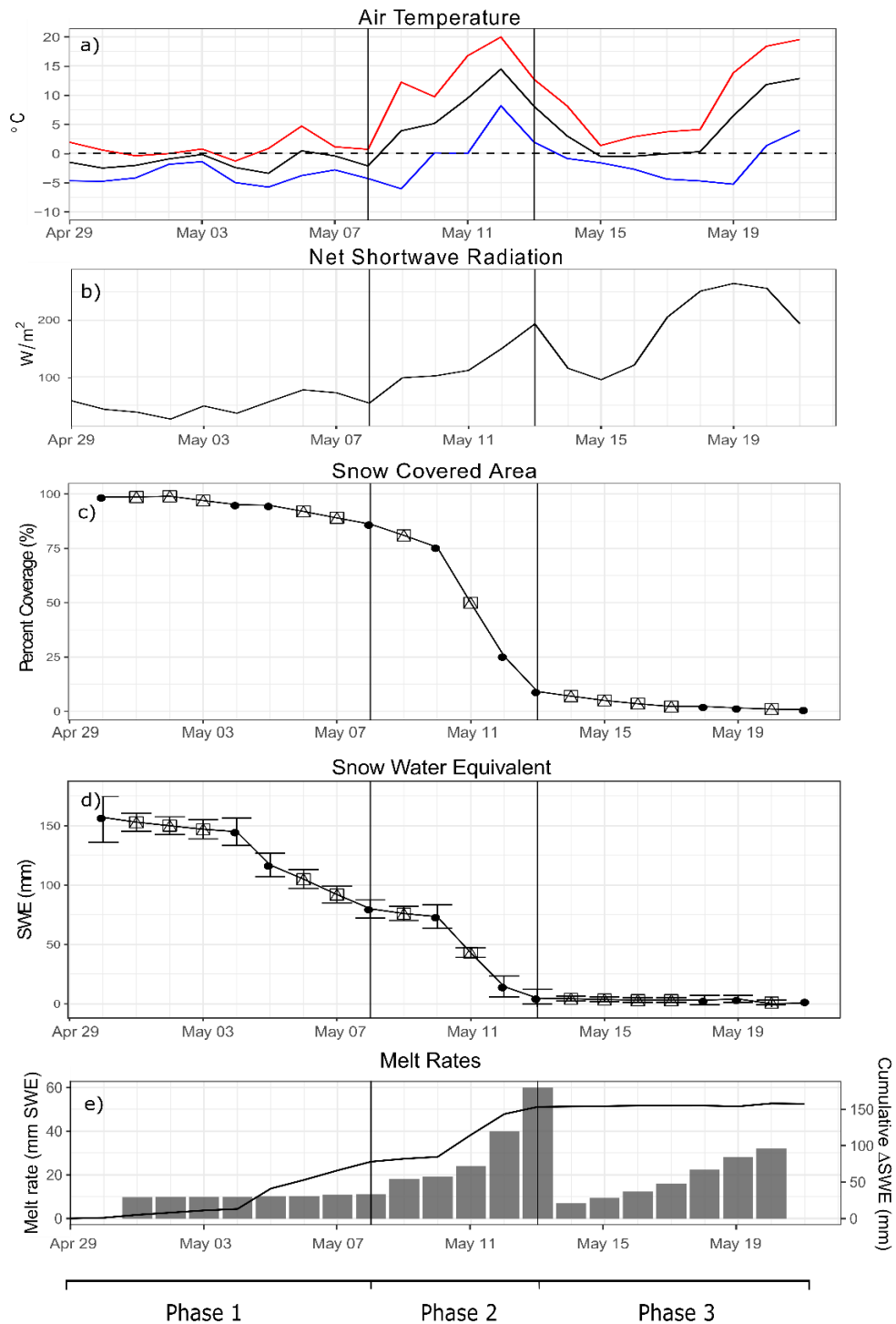
Figure 2-10: Daily a) air temperature, b) average net shortwave radiation, c) snow covered area, d) basin SWE presented with error bars. Circles are UAS derived SWE, Boxes are interpolated SWE averages. e) Daily melt rates per unit snow covered area (left) and cumulative (right) for each date. Lines delineate the three phases of the 2016 spring snowmelt. Stream discharge did not occur until 08 May.

deposited over the winter months. Between 13 May and 21 May the catchment was

characterized by a slow decline in SWE of ~5 mm (5 to <1mm respectively) while SCA

decreased by 8% over the eight day period. Due to meteorological conditions and the

relatively small portion of remaining snow this phase is characterized by slow declines

in SWE and SCA with slightly larger daily melt rates for the remaining snowcover

ranging averaging 22 mm/day. Marsh and Pomeroy (2006) showed melt rates varying

from 5 to 50 mm of melt per day during the later portion of the melt in 1993. Again,

although not directly comparable, this study provides similar melt estimates from the

model as to those presented in this paper suggesting that the melt rates estimated from

the UAS fall within an expected range. Only trace amounts of snow remain located on

steep north-east facing slopes remain after the final UAS flight on 21 May. Anecdotal

observations show these drifts remaining into late June.

Snow depletion curve

A snow depth depletion curve was fit for the 2016 UAS estimated SCA and SWE

(Figure 2-11) revealing the non-linear relationship between basin SWE and SCA while

highlighting the three distinct melt phases. As seen in previous studies (Pohl and Marsh,

2006; Pomeroy et al., 2006; Quinton and Carey, 2008) an analysis of the snowmelt

reveals a spatially heterogeneous melt primarily caused by spatial variations in

incoming solar radiation, or lack thereof, further controlled by slope, aspect and

vegetation shading. Across the study area we observe the shallow snowpacks begin to

melt out at an earlier date, particularly in areas with slopes with south-west aspects as

they are expected to receive a relatively large amount of incoming solar radiation.

Variations in melt rates by slope and aspect are not addressed directly in this study,

however spatially distributed SWE estimates presented in Figure 2-9 demonstrate these trends. Localized melt patterns across the landscape resulted in meltwater runoff towards the stream channel, however no hydrograph response was observed until 08 May suggesting that a large quantity of the initial SWE (7

7 mm) had melted and was being stored in the remaining snowpack as it made is way towards the basin outlet thus highlighting a significant lag between meltwater production and streamflow runoff. Further analysis is required to better understand the complex processes occurring over the snowmelt period. Data-driven results presented in this paper may lead to improved understanding of these processes and contribute to improved modelling capacities.
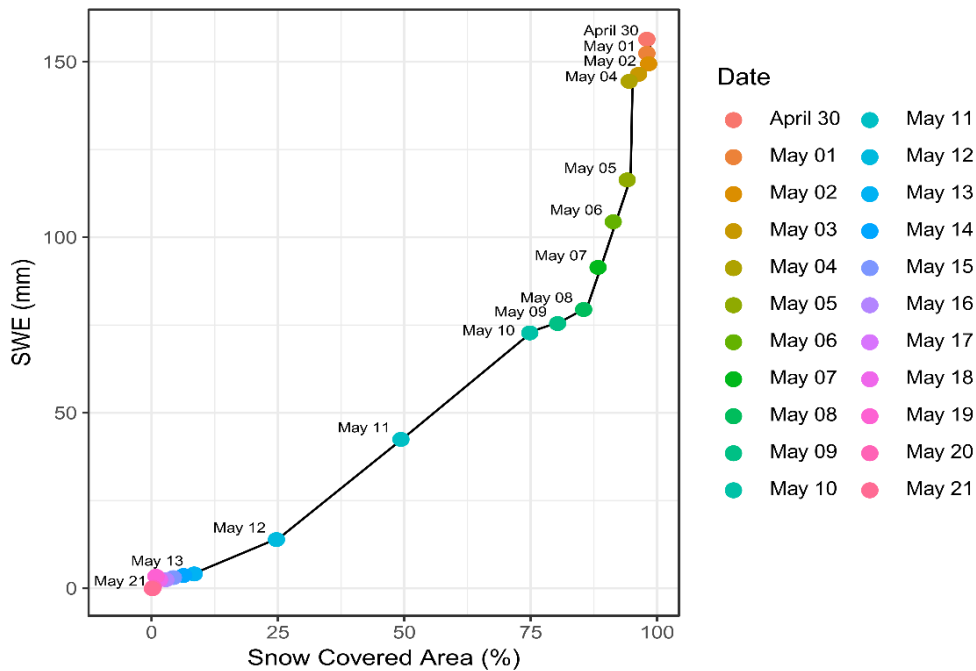
Figure 2-11: Snow depletion curve for Siksik Creek catchment over the 2016 spring snowmelt. Basin average SWE (x-axis) and snow covered area (y-axis) are derived using UAS. Coloured dots correspond to the date each variable was estimated.

Landscape variations in SCA and SWE

High resolution spatio-temporal snow covered area and water equivalent produced from the UAS enable a further analysis of snowpack changes by landcover type, highlighting the importance of spatially distributed snowmelt patterns influenced by vegetation cover and end-of-winter snow distribution. Here we focus on localized changes to SCA and SWE to understand snow ablation timing and magnitude across the three melt phases. Figure 2-12a shows temporal decline in SCA the four dominant land cover types found in the study watershed. Notable here is the initial decline in SCA for short shrubs between 05-09 May showing a 33% decline. During this time the remainder of the basin experiences smaller declines in SCA (16%, 6% and 10% for tundra, tall shrub, and drift respectively). Short shrub regions, characterized by shallow initial snow depths and slopes whose aspect are favourable towards increased incoming solar radiation (south and south-west facing), feature large melt rates during the initial phase of the melt. The rapid decline in SCA and SWE for short shrub regions early in the spring is likely responsible for a significant portion of the large decline in basin SWE observed during Phase 1 of the melt. The initial decline in SCA for short shrubs is followed closely by tundra on 10 May. In contrast, a slow decline in SCA for tall shrub and drift areas was observed over the spring melt period and both land units containing snowcover (<5% SCA) beyond the study period of interest. By 18 May most of the snowcover had ablated, marked by a 2% total basin SCA. However, at this time drifts remained 13% snow-covered.

To better contextualize the relative importance of SCA decline by landcover type, SCA for each of the four landcover units was plotted as a proportion of the total

remaining SCA (Figure 2-12b). To ensure estimates of proportional SCA were equal to the basin SCA tall shrub and drift regions were considered mutually exclusive. During the initial phase of the melt, tundra accounts for over 50% of the remaining snowcover. However, as SCA declines tundra contributes less to the remaining snowpack as these areas with shallow snowpacks, covering a large spatial area, become snow free. Towards the end of Phase 2 we observe a transition towards snow covered areas dominated by deeper snowpacks associated with tall shrub and drift features as these are the only areas with remaining snow. 18 May shows over 78% of the remaining SCA is contained in tall shrub and drift areas (53% and 25% respectively) with only 22% of the remaining 2% basin SCA in tundra and short shrub areas. Although this makes up a small fraction of the total basin SCA it is still important as the timing of snow cover depletion can have important implications on soil temperatures, active layer development, vegetation, and runoff pathways (Endrizzi et al., 2011; Lantz et al., 2013; Myers-Smith et al., 2015; Quinton and Carey, 2008).

Figure 2-12c reveals variations in SWE across the melt period by landcover type. At the onset of melt a significant portion of the total SWE is contained within the tundra regions, accounting for 41% of the total remaining SWE (Figure 2-12d), followed by 28% in tall shrubs, 17% in short shrub and 14% in large topographic drifts, with the latter contributing only 6% to the total basin area. Relative snow storage at the peak of the melt (12 May) is characterized by a shift from initially low SWE, as found in shallow tundra and shrub patches (81% the combined basin area), towards an emergence of deeper snowpacks found in tall shrub and drift areas (19% of the basin area) containing the majority of the remaining SWE. This is expected as snow ablation during the second

melt phase, associated with warming temperatures and high melt rates, results in a complete ablation of short shrub and tundra snowpacks characterized by initially low SWE values. However, in contrast to previous studies (Marsh et al., 2010; Pomeroy et al., 2006) who demonstrate larger melt rates and earlier melt completion for tall shrub sites, this study concludes that tall shrub patches did not feature earlier snowmelt completion dates and contain both relatively large SCA and SWE late into the melt period. The high-resolution spatial data obtained via UAS allows for the documentation of transition where the majority of the remaining SWE is contained in the tall shrub and drift areas (Figure 2-12d), after which the majority of SWE available to the hydrological system as meltwater runoff is assumed to be sourced from these areas of the basin. A summary of the snowpack conditions for select key dates is presented in Table 3 highlighting changes in snow covered area, water storage, and remaining SWE for each individual area.

Spatial data (Figure 2-9) obtained by the UAS reveals tundra and short shrub regions, particularly those found on south and west facing slopes, feature initially low SWE values and were observed snow-free approximately 10 days earlier than those snowpacks with a higher initial SWE. This is in agreement with previous studies (Marsh et al., 2008, 2010; Marsh and Pomeroy, 1996; Pomeroy et al., 2006) who demonstrated the shallower snowpacks associated with these land cover types fully contribute their initial SWE as runoff at earlier dates. However, these studies fail to provide frequent observations of the spatial heterogeneity of the snowmelt and rely on infrequent observations and physically based models to address these issues. This highlights a

key advantage to the UAS method for measuring SCA and SWE as it provides the

necessary data to address such issues.
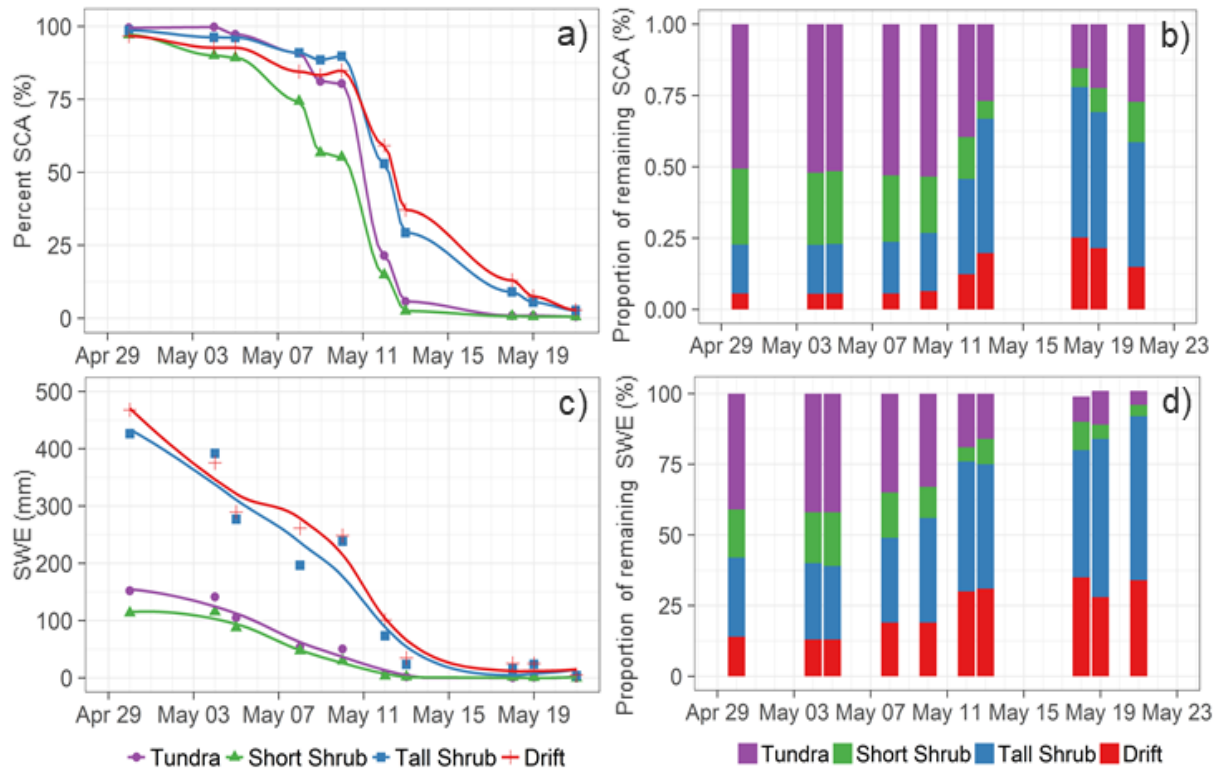
Figure 2-12: a) Decline in snow covered area by land unit, b) Proportional snow covered area by land units relative to the remaining SCA during the study period. c) SWE by land unit normalized to land unit area. Lines plotted with linear smoothing function (LOESS in R) added to display, d) Proportional snow water storage remaining by land unit classified as percent of remaining snow water storage.

Table 3: Snow characteristics summary by land unit for Siksik creek catchment area over the duration of the 2016 spring snowmelt.

April 30th

	Area (m²)	SCA (%)	Water Storage (m³)	Percent Water Storage (%)	SWE (mm)
Tundra	438,727	99	66,778	41	152
Short Shrub	235,764	97	26,761	17	114
Tall Shrub	103,892	98	44,277	28	294
Drift	49,546	97	23,178	14	468
Total		99	139,788		157

May 5th

	Area (m²)	SCA (%)	Water Storage (m³)	Percent Water Storage (%)	SWE (mm)
Tundra	438,727	97	46,097	46	105
Short Shrub	235,764	89	20,651	21	88
Tall Shrub	103,892	94	19,598	19	189
Drift	49,546	93	14,355	14	290
Total		95	96,811		117

May 8th

	Area (m²)	SCA (%)	Water Storage (m³)	Percent Water Storage (%)	SWE (mm)
Tundra	438,727	91	23,650	42	54
Short Shrub	235,764	74	11,209	20	48
Tall Shrub	103,892	91	14,391	25	197
Drift	49,546	84	7,328	13	261
Total		86	57,095		80

May 12th

	Area (m²)	SCA (%)	Water Storage (m³)	Percent Water Storage (%)	SWE (mm)
Tundra	438,727	21	3,105	26	7
Short Shrub	235,764	15	831	7	4
Tall Shrub	103,892	32	3,215	26	74
Drift	49,546	59	5,011	41	101
Total		25	11,969		14

May 13th

	Area (m²)	SCA (%)	Water Storage (m³)	Percent Water Storage (%)	SWE (mm)
Tundra	438,727	6	908	16	2
Short Shrub	235,764	2	501	9	2
Tall Shrub	103,892	29	2,457	44	24
Drift	49,546	37	1,735	31	35
Total		9	3,859		5

May 18th

	Area (m²)	SCA (%)	Water Storage (m³)	Percent Water Storage (%)	SWE (mm)
Tundra	438,727	1	327	9	1
Short Shrub	235,764	1	360	10	2
Tall Shrub	103,892	9	1,623	45	16
Drift	49,546	13	1,261	35	25
Total		2	2,246		3

Discussion

Effects of vegetation on snowmelt

Numerous studies have addressed the mechanisms behind shrub proliferation in tundra environments (Lantz et al., 2013; Myers-Smith et al., 2015; Racine et al., 2001; Sturm et al., 2001). A well-accepted snow-shrub hypothesis proposed by Myers-Smith *et al.* (2011) suggests a positive feedback mechanism for further shrub proliferation driven by a warming climate. In this hypothesis further shrub growth is a result of increased soil temperatures driven by increasing snow accumulation within shrub patches. Many studies have focussed on shrub expansion into the tundra with relation to increasing snow accumulation (Liston et al., 2002; McFadden et al., 2001; Sturm et al., 2005), but interactions between shrub proliferation and snowmelt hydrology remain unknown due to the complex interactions of vegetation on snow accumulation and melt rates.

Analysis of high-resolution SCA and SWE allows for the influences of vegetation cover on the timing and magnitude of shrub tundra snowmelt to be addressed through direct observations, raising interesting questions regarding changes to the spring hydrology of tundra systems with further climate-related changes. It is clear there is an association between vegetation cover and snow distribution across the landscape, as confirmed by past research (Mann, 2018; Marsh et al., 2008; McFadden et al., 2001; Rees et al., 2014), but what remains unknown is exactly how future vegetation changes will affect the distribution of snowcover in tundra environments, and how this will influence the timing and magnitude of snowmelt and the spring freshet. In this study, landscape controls on snowmelt patterns demonstrate the importance of large tall shrub

patches for affecting the landscape distribution of snow, resulting in delayed snowmelt runoff timings. These results contradict previous studies who found that tall shrub patches feature earlier snowmelt completion dates despite having a larger initial SWE (Marsh et al., 2010; Pomeroy et al., 2006). For example, Marsh *et al.* (2008) observed end-of-winter SWE in tall shrub patches at Trail Valley Creek to be 40% greater than the surrounding tundra regions but found rapid declines in SWE and SCA suggesting faster melt rates. This study also observed a faster decline in SWE for tall shrubs but found the SCA declined much slower than surrounding tundra and short shrub patches suggesting mixed results in comparison to previous work. One explanation for this could be that most of the tall shrub patches consisted of buried shrubs within the snowpack and therefore do not feature the same characteristics as the shrubs in these studies. Recent studies by Sturm *et al.* (2005), Pomeroy *et al.* (2006) and Marsh *et al.* (2010), have found the bending and burial of shrubs can reduce surface albedo and lower heat energy transfers into the snowpack that would otherwise expediate the melt rates. These studies primarily focussed on the influence of tall shrubs exceeding 1.5 m in height, but as presented in this study, short shrubs (<1 m) that are buried in the snowpack are also important for understanding snowmelt timing and snowpack ablation, especially during Phase 1 of the melt.

The effects of tall shrubs on snow distribution and melt have been well studied (Domine et al., 2016; Lantz et al., 2013; Marsh et al., 2008; Sturm et al., 2001), but the impacts of short shrubs on snow accumulation and melt timing is less documented in the literature. In this study short shrub patches were characterized by the most rapid decline in SCA and featured the earliest snowmelt completion. At the onset of the melt,

these patches featured similar end-of-winter SWE to tundra, however experienced

earlier declines in SCA and SWE. This is thought to be a result of the westward facing

slopes that allow for maximum incoming solar radiation as the days become longer and

the incoming shortwave radiation increases. This is in combination with localized melt

caused by emergence of the short shrub canopy after initial declines in snow depth.

Anecdotal evidence from the 2016 spring melt suggest once the snowpack declines

slightly, short shrubs *(B. Nana* primarily*)* began to protrude above the snow surface, a

phenomenon which led to a rapid localized melt as the shrub branches transfer energy

into the surrounding snowpack. Similar observations were reported by Pomeroy *et al.*

(2006) for both short and tall shrubs following the emergence of buried branches above

the snowpack. This was observed to result in greater transfers of energy into the

snowpack causing localized snowmelt from within the snowpack. The transfer of energy

into the snowpack combined with shallow initial snow depths and favourable aspect

may be responsible for the observed rapid snow ablation in these areas. It is unclear

how future expansion of short and tall shrubs will effect the tundra snow distribution and

snowmelt timing, citing the need for further research and improvement of current

hydrological models.

Unmanned Aerial System applications for Snow Hydrology

Spatial heterogeneity of tundra snowmelt has been documented by numerous

studies (Busseau et al., 2017; Davison et al., 2006; Marsh et al., 2008; Pohl and Marsh,

2006), however they are limited by a lack of appropriate high-resolution observations,

and instead rely on a combination of end-of-winter terrain based snow surveys and melt

models to predict landscape changes in snowmelt and runoff. These methods are prone

to larger errors and rely on the ability to accurately capture the heterogeneity of snow across multiple scales. Current methods for mapping SWE using traditional snow surveys and remote sensing methods, such as radar or airborne lidar, attempt to address this but often fail to capture both the wide range of snow depths and the fine-scale spatial variability found in the Arctic tundra. Furthermore, these methods present issues when measuring snow depth, density, SWE and SCA at catchment scales with adequate repeat data collection.

Recent studies Shi et al. (2015) and Musselman et al. (2017) reveal a knowledge gap in future changes to the snowmelt timing under further climate warming scenarios and stress the need for enhanced monitoring of Arctic environments to better understand and predict changes to the hydrological systems. This can only be accomplished through the application of advanced fine-scale physically based hydrological models, however current models tend to fail at accurately modelling the spring snowmelt period and freshet. In this paper we address this lack of high-resolution spatial and temporal data through providing micro-scale measurements of both SCA and SWE over the duration of the spring melt using UAS. The SfM photogrammetry technique allowed for high-resolution measurements of snow depth and SCA with the input of spatially distributed snowpack densities. By integrating manual observations of snowpack density with remotely sensed UAS snow depth data we were able to produce estimates of SWE at fine spatio-temporal resolutions. This paper addresses one of the primary issues faced by the hydrological modelling community; capturing the spatial and temporal heterogeneity of the landscape (Clark et al., 2017; Peters-Lidard et al., 2017), emphasizing an urgent need to use tools such as UAS to validate these models. We

provide an unprecedented overview of the spring snowmelt for tundra environments that will enable the modelling community to test hydrological models without reliance on point scale observations of snow covered area, water equivalent and storage, and melt rates.

Limitations of Unmanned Aerial Systems for estimating Snow Water Equivalent

Challenges relating to SWE retrieval using remote sensing methods have historically proven difficult for hydrologists and remote sensors alike. Many remote sensing techniques have been developed for SWE retrieval relying on passive or active radar (Dietz et al., 2012) and airborne lidar (Painter et al., 2016). These techniques have demonstrated great success, however they often feature a coarse spatial and/or temporal resolution and are best suited for broad regional scales. The UAS SWE estimates presented attempts to bridge the gap between point observations and broad remote sensing and may lead to improvement of these techniques through creating of improved validation datasets. However, as with all remote sensing of SWE methodologies the UAS SfM method is not without limitations, resulting from inference of SWE from snow depth and density estimates. As an example, The *Airborne Snow Observatory (ASO)* (Painter et al., 2016) represents one of the first operational airborne retrieval of repeat SWE observations over the snowmelt albeit across much larger scales than presented in this study. The ASO utilizes airborne lidar estimates of snow depths for the Sierra Nevada mountain range in combination with modelled snowpack density using a physically-based energy-balance model. The input of spatially distributed snow density enables researchers to estimate SWE at large catchment scales over the snowmelt, however spatially distributed snow density estimates have

been cited as a primary source of uncertainty for SWE retrieval. In this study we incorporate in-situ observations of snow density by creating a simple linear relationship with snow depth in attempt to capture spatially distributed density and SWE. This proved effective at representing spatial variations across the study area but could certainly be improved upon using spatially distributed modelled or measured snowpack density measurements. UAS estimates of SWE are heavily dependant on accurately measuring snow depth and density. Future work is needed to reduce uncertainty in both snow depth and spatially-distributed snowpack density to further improve the accuracy of UAS as a snow hydrology tool.

Conclusion

This study demonstrates the successful application of Unmanned Aerial Systems for measuring high spatial and temporal changes in snow water equivalent (SWE) and snow covered area (SCA) for a shrub-tundra headwater basin. Measuring SWE across the basin is dependent on combining accurate snow depth SfM maps with distributed snow densities. To address spatial and temporal changes in snowpack density we applied observations of measured snowpack density to create snow depth-density rating curves across the melt period removing the reliance on modelled snowpack densities to produce SWE maps.

High-resolution changes to SCA and SWE were documented with unprecedented temporal distribution to provide insights on the micro-scale changes in SCA, SWE, and snowmelt patterns across the rapid spring melt. In this study three primary phases are observed over the course of the spring melt. These are characterized by 1) low melt rates across a large area resulting in a large decline in SWE with minor change in SCA,

79

2) high melt rates resulting in drastic declines in both SCA and SWE, and 3) low melt rates over a small portion of the basin, resulting in little change to either SCA or SWE as the only remaining snowpack is located in large drift regions. The remote sensing technique applied using UAS allowed for observations of basin average melt rates rather than relying on estimations via snowmelt models. This allows for an understanding of changes to the catchment snow storage and will provide valuable information to future hydrological applications.

Further analysis of spatial changes to the snowpack by land cover type highlight the importance of capturing small-scale heterogeneity across the snowmelt. Spatio-temporal analysis of the snowmelt highlights the importance of vegetation and snow distribution on snowmelt ablation, whereby shallow snowpacks found in tundra and short shrub areas feature notably earlier snowmelt declines, and tall shrub and drift snowpacks contain a large relative quantity of snow late into the melt period. This may have important hydrological implications for snowmelt water runoff, spring freshet timing and magnitude, and soil temperatures and active-layer development. Snowcover conditions presented in this study allow micro-scale changes in snow water equivalent and covered area to be documented at unprecedented scales, providing a valuable tool for future hydrological studies and improvement of hydrological models.

The UAS method for analysing the distribution of snow depth, SCA and SWE demonstrates multiple advantages over other remote sensing techniques such as airborne campaigns and in-situ snow surveys at catchment scales. The observed rapid 2016 snowmelt season highlights the importance of collecting high-resolution spatial data and demonstrates the need for data collection at regular intervals across the melt,

as changes to the landscape snow cover can occur drastically over a period of a few days. Results of this study provide insights into the spring snowmelt patterns of shrub-tundra catchments and provide important data-driven outputs that will be valuable for improving and validation of hydrological models.

References

Berezovskaya, S., Kane, D.L., 2007. Measuring snow water equivalent for hydrological applications: part 1, accuracy of observations. 16th Int. North. Res. Basins Symp. Work. 29–35.

Bühler, Y., Adams, M.S., Bosch, R., Stoffel, A., 2016. Mapping snow depth in alpine terrain with unmanned aerial systems (UASs): Potential and limitations. Cryosphere 10, 1075–1088. https://doi.org/10.5194/tc-10-1075-2016

Bühler, Y., Adams, M.S., Stoffel, A., Boesch, R., 2017. Photogrammetric reconstruction of homogenous snow surfaces in alpine terrain applying near-infrared UAS imagery. Int. J. Remote Sens. 38, 3135–3158. https://doi.org/10.1080/01431161.2016.1275060

Busseau, B.C., Royer, A., Roy, A., Langlois, A., Domine, F., 2017. Analysis of snow-vegetation interactions in the low Arctic-Subarctic transition zone (northeastern Canada). Phys. Geogr. 38, 159–175. https://doi.org/10.1080/02723646.2017.1283477

Clark, M.P., Hendrikx, J., Slater, A.G., Kavetski, D., Anderson, B., Cullen, N.J., Kerr, T., Örn Hreinsson, E., Woods, R. a., 2011. Representing spatial variability of snow water equivalent in hydrologic and land-surface models: A review. Water Resour. Res. 47, 1–23. https://doi.org/10.1029/2011WR010745

Colomina, I., Molina, P., 2014. Unmanned aerial systems for photogrammetry and remote sensing: A review. ISPRS J. Photogramm. Remote Sens. 92, 79–97. https://doi.org/10.1016/j.isprsjprs.2014.02.013

Davison, B., Pohl, S., Dornes, P., Marsh, P., Pietroniro, A., MacKay, M., 2006. Characterizing snowmelt variability in a land-surface-hydrologic model. ATMOSPHERE-OCEAN 44, 271–287. https://doi.org/10.3137/ao.440305

De Michele, C., Avanzi, F., Passoni, D., Barzaghi, R., Pinto, L., Dosso, P., Ghezzi, A., Gianatti, R., Vedova, G. Della, 2016. Using a fixed-wing UAS to map snow depth distribution: An evaluation at peak accumulation. Cryosphere 10, 511–522. https://doi.org/10.5194/tc-10-511-2016

DeBeer, C.M., Pomeroy, J.W., 2010. Simulation of the snowmelt runoff contributing area in a small alpine basin. Hydrol. Earth Syst. Sci. 14, 1205–1219. https://doi.org/10.5194/hess-14-1205-2010

Deems, J.S., Painter, T.H., Finnegan, D.C., 2013. Lidar measurement of snow depth: A review. J. Glaciol. 59, 467–479. https://doi.org/10.3189/2013JoG12J154

Dixon, D., Boon, S., 2012. Comparison of the SnowHydro snow sampler with existing snow tube designs. Hydrol. Process. 26, 2555–2562. https://doi.org/10.1002/hyp.9317

Endrizzi, S., Quinton, W.L., Marsh, P., 2011. Modelling the spatial pattern of ground thaw in a small basin

in the arctic tundra. Cryosph. Discuss. 5, 367–400. https://doi.org/10.5194/tcd-5-367-2011

Goodison, B., Louie, P.Y.T., Yang, D., 1998. WMO solid precipitation measurement intercomparison. Final Rep. 318.

Goodison, B.E., Glynn, J.E., Harvey, K.D., Slater, J.E., 1987. Snow Surveying in Canada: A Perspective. Can. Water Resour. J. 12, 27–42. https://doi.org/10.4296/cwrj1202027

Harder, P., Schirmer, M., Pomeroy, J., Helgason, W., 2016. Accuracy of snow depth estimation in mountain and prairie environments by an unmanned aerial vehicle. Cryosphere 10, 2559–2571. https://doi.org/10.5194/tc-10-2559-2016

Heginbottom, J.A., Radburn, L.K., 1992. Permafrost and ground ice conditions of northwestern Canada; Geological Survey of Canada, Map 1691A, scale 1:1,000,000.

Hopkinson, C., Pietroniro, A., Pomeroy, J.W., 2008. Hydroscan: airborne laser mapping of hydrological features and resources.

Lantz, T.C., Marsh, P., Kokelj, S. V., 2013. Recent Shrub Proliferation in the Mackenzie Delta Uplands and Microclimatic Implications. Ecosystems 16, 47–59. https://doi.org/10.1007/s10021-012-9595-2

Liston, G.E., Mcfadden, J.P., Sturm, M., Pielke, R. a, 2002. Modelled changes in arctic tundra snow, energy and moisture fluxes due to increased shrubs. Glob. Chang. Biol. 8, 17–32. https://doi.org/10.1046/j.1354-1013.2001.00416.x

Macdonald, J., Pomeroy, J., 2007. Gauge Undercatch of Two Common Snowfall Gauges in a Prairie Environment. Proc. 64th East. Snow Conf. St. John's, Canada. 119–126.

Mann, P., 2018. Spatial and temporal variability of the snow environment in the Western Canadian Arctic. Wilfrid Laurier University.

Marks, D., Dozier, J., 1992. Climate and energy exchange at the snow surface in the Alpine Region of the Sierra Nevada: 2. Snow cover energy balance. Water Resour. Res. 28, 3043–3054. https://doi.org/10.1029/92WR01483

Marsh, P., 1987. Grain growth in a wet arctic snow cover. Cold Reg. Sci. Technol. 14, 23–31. https://doi.org/10.1016/0165-232X(87)90041-3

Marsh, P., Bartlett, P., MacKay, M., Pohl, S., Lantz, T., 2010. Snowmelt energetics at a shrub tundra site in the western Canadian Arctic. Hydrol. Process. 24, 3603–3620. https://doi.org/10.1002/hyp.7786

Marsh, P., J. Pomeroy, S. Pohl, W. Quinton, C. Onclin, M. Russell, N. Neumann, A. Pietroniro, B. Davison, S. McCartney, 2008. Snowmelt processes and runoff at the Arctic treeline: Ten years of MAGS Research. Cold Reg. Atmos. Hydrol. Stud. Mackenzie GEWEX Exp. Volume 2:, 97–124.

Marsh, P., Pomeroy, J.W., 1996. Meltwater fluxes at an arctic forest-tundra site. Hydrol. Process. 10, 1383–1400. https://doi.org/10.1002/(SICI)1099-1085(199610)10:10<1383::AID-HYP468>3.0.CO;2-W

Marsh, P., Pomeroy, J.W., Neumann, N., 1997. Sensible heat flux and local advection over a heterogeneous landscape at an Arctic tundra site during snowmelt. Ann. Glaciol. 25, 132–136.

Marsh, P., Quinton, W.L., Pomeroy, J.W., 1995. Hydrological Processes and Runoff at the Arctic Treeline in Northwestern Canada. 10th Annu. North. Basins Symp. 368–397.

Marsh, P., Woo, M.-K., 1984. Wetting Front Advance and Freezing of Meltwater Within a Snow Cover 1. Observations in the Canadian Arctic. Water Resour. Res. 20, 1853–1864.

Marsh, P., Woo, M., 1981. Snowmelt, glacier melt, and high arctic streamflow regimes. Can. J. Earth Sci. 18, 1380–1384. https://doi.org/10.1139/e81-127

McFadden, J.P., Liston, G.E., Sturm, M., Pielke, R. a., Chapin, F.S., Pielke SR, R., Chapin III, S., 2001. Interactions of shrubs and snow in arctic tundra: measurements and models, in: Soil Vegetation-Atmosphere Transfer Schemes and Large-Scale Hydrological Models. IAHS Publ. No. 270. pp. 317–325.

Myers-Smith, I.H., Elmendorf, S.C., Beck, P.S.A., Wilmking, M., Hallinger, M., Blok, D., Tape, K.D., Rayback, S.A., Macias-Fauria, M., Forbes, B.C., Speed, J.D.M., Boulanger-Lapointe, N., Rixen, C., Lévesque, E., Schmidt, N.M., Baittinger, C., Trant, A.J., Hermanutz, L., Collier, L.S., Dawes, M.A., Lantz, T.C., Weijers, S., JØrgensen, R.H., Buchwal, A., Buras, A., Naito, A.T., Ravolainen, V., Schaepman-Strub, G., Wheeler, J.A., Wipf, S., Guay, K.C., Hik, D.S., Vellend, M., 2015. Climate sensitivity of shrub growth across the tundra biome. Nat. Clim. Chang. 5. https://doi.org/10.1038/nclimate2697

Myers-Smith, I.H., Forbes, B.C., Wilmking, M., Hallinger, M., Lantz, T., Blok, D., Tape, K.D., MacIas-Fauria, M., Sass-Klaassen, U., Lévesque, E., Boudreau, S., Ropars, P., Hermanutz, L., Trant, A., Collier, L.S., Weijers, S., Rozema, J., Rayback, S.A., Schmidt, N.M., Schaepman-Strub, G., Wipf, S., Rixen, C., Ménard, C.B., Venn, S., Goetz, S., Andreu-Hayles, L., Elmendorf, S., Ravolainen, V., Welker, J., Grogan, P., Epstein, H.E., Hik, D.S., 2011. Shrub expansion in tundra ecosystems: Dynamics, impacts and research priorities. Environ. Res. Lett. 6. https://doi.org/10.1088/1748-9326/6/4/045509

Nolan, M., Larsen, C., Sturm, M., 2015. Mapping snow-depth from manned-aircraft on landscape scales at centimeter resolution using Structure-from-Motion photogrammetry. Cryosph. Discuss. 9, 333–381. https://doi.org/10.5194/tcd-9-333-2015

Painter, T.H., Berisford, D.F., Boardman, J.W., Bormann, K.J., Deems, J.S., Gehrke, F., Hedrick, A., Joyce, M., Laidlaw, R., Marks, D., Mattmann, C., McGurk, B., Ramirez, P., Richardson, M., Skiles, S.M.K., Seidel, F.C., Winstral, A., 2016. The Airborne Snow Observatory: Fusion of scanning lidar, imaging spectrometer, and physically-based modeling for mapping snow water equivalent and snow

albedo. Remote Sens. Environ. 184, 139–152. https://doi.org/10.1016/j.rse.2016.06.018

Pan, X., Yang, D., Li, Y., Barr, A., Helgason, W., Hayashi, M., Marsh, P., Pomeroy, J., Janowicz, R.J., 2016. Bias corrections of precipitation measurements across experimental sites in different ecoclimatic regions of western Canada. Cryosphere 10, 2347–2360. https://doi.org/10.5194/tc-10-2347-2016

Peters-Lidard, C.D., Clark, M., Samaniego, L., Verhoest, N.E.C., Van Emmerik, T., Uijlenhoet, R., Achieng, K., Franz, T.E., Woods, R., 2017. Scaling, similarity, and the fourth paradigm for hydrology. Hydrol. Earth Syst. Sci. 21, 3701–3713. https://doi.org/10.5194/hess-21-3701-2017

Pohl, S., Marsh, P., 2006. Modelling the spatial-temporary variability of spring snowmelt in an arctic catchment. Hydrol. Process. 20, 1773–1792. https://doi.org/10.1002/hyp.5955

Pohl, S., Marsh, P., Liston, G.E., 2006. Spatial-temporal variability in turbulent fluxes during spring snowmelt. Arctic, Antarct. Alp. Res. 38, 136–146.

Pomeroy, J.W., Bewley, D.S., Essery, R.L.H., Hedstrom, N.R., Link, T., Granger, R.J., Sicart, J.E., Ellis, C.R., Janowicz, J.R., 2006. Shrub tundra snowmelt. Hydrol. Process. 20, 923–941. https://doi.org/10.1002/hyp.6124

Pomeroy, J.W., Gray, D.M., 1995. Snowcover accumulation, relocation and management, National Hydrological Research Institute Science Report No. 7. Saskatoon.

Pomeroy, J.W., Gray, D.M., Brown, T., Hedstrom, N.R., Quinton, W.L., Granger, R.J., Carey, S.K., 2007. The cold regions hydrological model : a platform for basing process representation and model structure on physical evidence. Hydrol. Process. 21, 2650–2667. https://doi.org/10.1002/hyp

Pomeroy, J.W., Hedstrom, N., Parviainen, J., 1999. The Snow Mass Balance of Wolf Creek , Yukon : Effects of Snow Sublimation and Redistribution. Wolf Creek Res. Basin Hydrol. Ecol. Environ. 15–30.

Pomeroy, J.W., Marsh, P., D.M. Gray, 1997. Application of a distributed blowing snow model to the Arctic. Hydrol. Process. 11, 1451–1464. https://doi.org/10.1002/(SICI)1099-1085(199709)11:11<1451::AID-HYP449>3.0.CO;2-Q

Prowse, T., Ommanney, S., 1990. Northern hydrology: Canadian perspectives. Environment Canada.

Quinton, W.L., Carey, S.K., 2008. Towards an energy-based runoff generation theory for tundra landscapes. Hydrol. Process. 22, 4649–4653. https://doi.org/10.1002/hyp.7164

Quinton, W.L., Carey, S.K., Goeller, N.T., 2004. Snowmelt runoff from northern alpine tundra hillslopes: major processes and methods of simulation. Hydrol. Earth Syst. Sci. 8, 877–890. https://doi.org/10.5194/hess-8-877-2004

Quinton, W.L., Marsh, P., 1999. A conceptual framework for runoff generation in a permafrost

environment. Hydrol. Process. 13, 2563–2581. https://doi.org/10.1002/(SICI)1099-1085(199911)13:16<2563::AID-HYP942>3.0.CO;2-D

Quinton, W.L., Marsh, P., 1998a. Meltwater fluxes, hillslope runoff and stream flow on an arctic permafrost basin. Permafrost, - 7th Int. Conf. Yellowknife (Canada), Collect. Nord. 921–926.

Quinton, W.L., Marsh, P., 1998b. The influence of mineral earth hummocks on subsurface drainage in the continuous permafrost zone. Permafr. Periglac. Process. 9, 213–228. https://doi.org/10.1002/(SICI)1099-1530(199807/09)9:3<213::AID-PPP285>3.0.CO;2-E

Racine, C., Sturm, M., Tape, K., 2001. Climate change: Increasing shrub abundance in the Arctic. Nature 411.

Raleigh, M.S., Small, E.E., 2017. Snowpack density modeling is the primary source of uncertainty when mapping basin-wide SWE with lidar. Geophys. Res. Lett. 44, 3700–3709. https://doi.org/10.1002/2016GL071999

Rees, A., English, M., Derksen, C., Toose, P., Silis, A., 2014. Observations of late winter Canadian tundra snow cover properties. Hydrol. Process. 28, 3962–3977. https://doi.org/10.1002/hyp.9931

Sevruk, B., Ondrás, M., Chvíla, B., 2009. The WMO precipitation measurement intercomparisons. Atmos. Res. 92, 376–380. https://doi.org/10.1016/j.atmosres.2009.01.016

Sexstone, G.A., Clow, D.W., Stannard, D.I., Fassnacht, S.R., 2016. Comparison of methods for quantifying surface sublimation over seasonally snow-covered terrain. Hydrol. Process. 30, 3373–3389. https://doi.org/10.1002/hyp.10864

Sivapalan, M., 2018. From engineering hydrology to Earth system science: Milestones in the transformation of hydrologic science. Hydrol. Earth Syst. Sci. 22, 1665–1693. https://doi.org/10.5194/hess-22-1665-2018

SnowHydro, 2013a. GPS Snow Depth Probe [WWW Document]. URL http://www.snowhydro.com/products/column2.html

SnowHydro, 2013b. SWE Coring Tube [WWW Document]. URL http://www.snowhydro.com/products/column3.html (accessed 7.11.18).

Sturm, M., Douglas, T., Racine, C., Liston, G.E., 2005. Changing snow and shrub conditions affect albedo with global implications. J. Geophys. Res. 110, G01004. https://doi.org/10.1029/2005JG000013

Sturm, M., Holmgren, J., Liston, G.E., 1999. Self-recording snow depth probe. 1741.

Sturm, M., Racine, C., Tape, K., 2001. Increasing shrub abundance in the Arctic. Nature 411.

Sturm, M., Taras, B., Liston, G.E., Derksen, C., Jonas, T., Lea, J., 2010. Estimating Snow Water Equivalent

Using Snow Depth Data and Climate Classes. J. Hydrometeorol. 11, 1380–1394. https://doi.org/10.1175/2010JHM1202.1

Thériault, J.M., Rasmussen, R., Ikeda, K., Landolt, S., 2012. Dependence of snow gauge collection efficiency on snowflake characteristics. J. Appl. Meteorol. Climatol. 51, 745–762. https://doi.org/10.1175/JAMC-D-11-0116.1

Vander Jagt, B., Lucieer, A., Wallace, L., Turner, D., Durand, M., 2015. Snow Depth Retrieval with UAS Using Photogrammetric Techniques. Geosciences 5, 264–285. https://doi.org/10.3390/geosciences5030264

Yang, D., Kane, D., Zhang, Z., Legates, D., Goodison, B., 2005. Bias corrections of long-term (1973-2004) daily precipitation data over the northern regions. Geophys. Res. Lett. 32, 1–5. https://doi.org/10.1029/2005GL024057

Young, K.L., Robert Bolton, W., Killingtveit, Å., Yang, D., 2006. Assessment of precipitation and snowcover in northern research basins. Nord. Hydrol. 37, 377. https://doi.org/10.2166/nh.2006.021

Chapter 3 : Conclusion and Final Remarks

This study applied high-resolution remote sensing of changes to the tundra snowcover across the spring snowmelt period. A fixed-wing Unmanned Aerial Systems (UAS) was used to map spatial and temporal changes to the snowpack for a shrub-tundra headwater catchment. This novel approach provides spatially distributed hydrological data directly addressing the current lack of information on small-scale heterogeneity of shrub-tundra snowmelt.

Chapter 2 provided an analysis of spatial and temporal changes in snow covered area (SCA) and snow water equivalent (SWE) across the spring melt for a <1 km^2 shrub-tundra headwater basin. Snow depth maps at 1 m resolution were created using UAS *Structure-from-Motion* (SfM) photogrammetry techniques and coupled with snow depth-density rating curves to produce estimates of SWE for 14 dates across the 2016 spring period. Changes to basin SCA and SWE were documented with unprecedented spatio-temporal resolution to provide insights on the micro-scale changes in SCA, SWE, and snowmelt patterns across the rapid spring melt. Analysis of basin-wide declines in SCA and SWE reveal three distinct melt phases characterized by 1) low melt rates across a large area resulting in a minor change in SCA, but a very large decline in SWE with, 2) high melt rates resulting in drastic declines in both SCA and SWE, and 3) low melt rates over a small portion of the basin, resulting in little change to either SCA or SWE.

A further analysis of SWE and SCA was undertaken based on four dominant land cover types (tundra, short shrub, tall shrub, and topographic snow drift) revealing trends in snowcover depletion by vegetation type, where shallow snowpacks found in tundra and short shrub regions feature notably earlier snowmelt declines. Findings also

demonstrate the importance of tall shrub and drift features that contain a large relative quantity of SWE late into the melt, featuring later melt completion dates by approximately 10 days.

Observed variations in snowmelt melt rates may have important implications to the hydrological regime of these environments and are integral for addressing unknowns with future changes to these environments. Future applications of datasets presented in this thesis will be valuable for improvement and validation of hydrological models leading to an improvement of our ability to predict snowpack distribution across tundra landscapes and enable hydrologists to better address the complex heterogeneity of snowmelt at landscape scales. The creation of high-resolution snowcover products presented in this study demonstrates the effectiveness of novel Unmanned Aerial Systems for snow hydrology.

High-resolution mapping of snow cover with UAS

The use of airborne imagery and remotely sensed data to determine snow covered area is the most common and effective method of creating a snow depletion curve, but the efficiency, accuracy, and precision of the Unmanned Aerial System makes this method more attractive for small-scale studies. The UAS platform provides high-resolution spatial information at daily, or sub-daily intervals with the potential for data acquisitions on an hourly scale if technological restraints were overcome. Our ability to capture such time sensitive landscape changes in the snowpack conditions using remote sensing, or traditional snow survey methods for that matter, is unprecedented and novel applications of UAS to snow hydrology lay the foundation for improved understanding of these complex environments.

One of the main benefits to the UAS, as highlighted in this thesis, is the ability to capture and document the rapidly changing snowmelt period. For instance, the rapid decline in snow covered area during the 2016 spring snowmelt saw catchment-wide decline in snow cover of 50% over just 3 days. Capturing rapid changes in SCA at catchment scales would have extremely difficult and expensive, if not impossible, using traditional methods. Another benefit to the UAS technique applied in this study over traditional remote sensing techniques lies in the ability to document changes to the snowcover of an entire catchment area at 1 m or less ground sampling distances, allowing the user to quantify changes at landscape scales with ease and accuracy without the need for expensive instruments and extensive airborne campaigns. This highlights a benefit for measuring SCA over traditional remote sensing techniques as the UAS imagery is not subject to atmospheric-related errors, primarily with regards to uncertainties relating to distinguishing between cloud and snow cover. A result of the relatively low flight altitude negates the need for atmospheric corrections in post-processing of the datasets as required by satellite derived snow covered area estimations (Rittger et al., 2013). Although not subject to atmospheric-related data issues the UAS is subject to weather conditions such as wind speed and lighting conditions. Such influences are evident in this study resulting in missing dates with UAS mapping over the duration of the melt period.

The main limitations of small UAS, such as the Sensefly eBee applied in this study, is the small aerial coverage, offering only practical applications for small-scale headwater catchment studies currently. The aerial coverage of such UASs is limited both by technological limitations, battery life for example, and current legal restrictions

for Canadian Unmanned Aerial Systems operators as set by Transport Canada (2018). Larger UAS exist but have many logistical and legal limitations that make their use impractical for research purposes, and are currently available to government organizations. However, it is expected that ongoing, and rapid, advances in UAS technology, combined with higher precision instrumentation and a wider platform of sensors will see the rise of Unmanned Aerial Systems applications for hydrology, enabling researchers to obtain high-resolution datasets over much larger areas and enable hydrologists to better address issues relating to scaling and capturing heterogeneity in hydrological models.

Future implications

Recent studies by Shi *et al.* (2015) and Musselman *et al.* (2017) demonstrate the complex nature of spring snowmelt hydrology and stress the need for enhanced monitoring of Arctic environments to better understand and predict changes to the hydrological systems. This can only be accomplished through the application of advanced fine-scale physically based hydrological models, however current models tend to fail at accurately modelling the spring snowmelt period and freshet, and once they are able to successfully model these conditions collecting high-resolution hydro-meteorological datasets will be the most valuable tool for validating and improving the models. One of the primary issues faced by the hydrological modelling community is capturing the spatial and temporal heterogeneity of the landscape (Clark et al., 2017; Peters-Lidard et al., 2017). Issues of scaling and heterogeneity complicate the ability to accurately represent the physical reality of hydrological factors. These issues were addressed in this study through the application of high spatial and temporal data

acquisition of the tundra snowcover through coupling of UAS SfM remote sensing and traditional snow survey observations. The need for high-resolution data to improve models has led hydrologists into the "fourth paradigm" of hydrology leading towards advances in data-driven knowledge (Peters-Lidard et al., 2017). The outcomes of this study are important for contributing to this data-driven "fourth-paradigm" in hydrology by contributing high-resolution tundra snow distributions, SWE, and spatio-temporal changes in snowmelt across the spring snowmelt- something that has previously been difficult at small catchment scales using traditional methods. Going forward this study will hopefully contribute to the modelling communities push to successfully validate high-resolution physically-based hydrological models' ability to capture localized snowmelt patterns and changes in SWE at small scales. Future coupling of high-resolution UAS remote sensing of snow, as presented here, with traditional hydrological measurements of eddy covariance evapotranspiration, stream discharge, and meteorological data will allow for a full documentation of the spring snowmelt hydrology for headwater tundra catchments and will help address the complex interactions between Arctic-tundra snowmelt and the spring freshet under future changing climate conditions.

References

Clark, M.P., Bierkens, M.F.P., Samaniego, L., Woods, R.A., Uijlenhoet, R., Bennett, K.E., Pauwels, V.R.N., Cai, X., Wood, A.W., Peters-Lidard, C.D., 2017. The evolution of process-based hydrologic models: Historical challenges and the collective quest for physical realism. Hydrol. Earth Syst. Sci. 21, 3427–3440. https://doi.org/10.5194/hess-21-3427-2017

Musselman, K.N., Clark, M.P., Liu, C., Ikeda, K., Rasmussen, R., 2017. Slower snowmelt in a warmer world. Nat. Clim. Chang. 7, 214–219. https://doi.org/10.1038/nclimate3225

Peters-Lidard, C.D., Clark, M., Samaniego, L., Verhoest, N.E.C., Van Emmerik, T., Uijlenhoet, R., Achieng, K., Franz, T.E., Woods, R., 2017. Scaling, similarity, and the fourth paradigm for hydrology. Hydrol. Earth Syst. Sci. 21, 3701–3713. https://doi.org/10.5194/hess-21-3701-2017

Rittger, K., Painter, T.H., Dozier, J., 2013. Assessment of methods for mapping snow cover from MODIS. Adv. Water Resour. 51, 367–380. https://doi.org/10.1016/j.advwatres.2012.03.002

Shi, X., Marsh, P., Yang, D., 2015. Warming spring air temperatures, but delayed spring streamflow in an Arctic headwater basin. Environ. Res. Lett. 10, 064003. https://doi.org/10.1088/1748-9326/10/6/064003

Transport Canada, 2018. Flying your drone safely and legally [WWW Document]. URL http://www.tc.gc.ca/en/services/aviation/drone-safety/flying-drone-safely-legally.html (accessed 7.12.18).

Appendix

Appendix 1: Climate normals for nearby Inuvik A (a) and Tuktoyaktuk (b) stations: 1981-2010. Daily min, max, and average temperature are shown as lines. Green bars are monthly average precipitation. Precipitation between October and April is primarily snow and accounts for over half the annual precipitation. Data obtained from Environment and Climate Change Canada (2018)
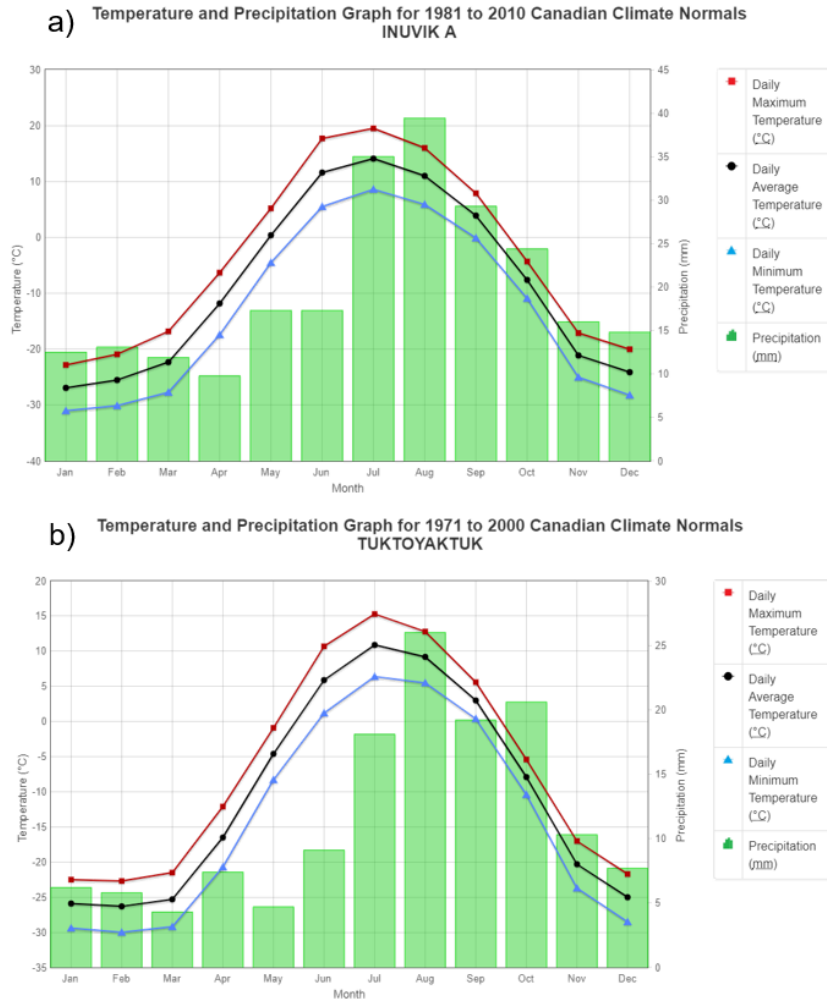
Source:

Environment and Climate Change Canada, 2018. Canadian Climate Normals 1981-2010 Station Data: Inuvik A [WWW Document]. URL http://climate.weather.gc.ca/climate_normals/results_1981_2010_e.html?stnID=1669&autofwd=1 (accessed 7.12.18).

Appendix 2: Specification summary for Sensefly EBEE Ag UAS applied in this study.
a) Sensefly EBEE Ag fixed wing UAV., b) UAS station in the field
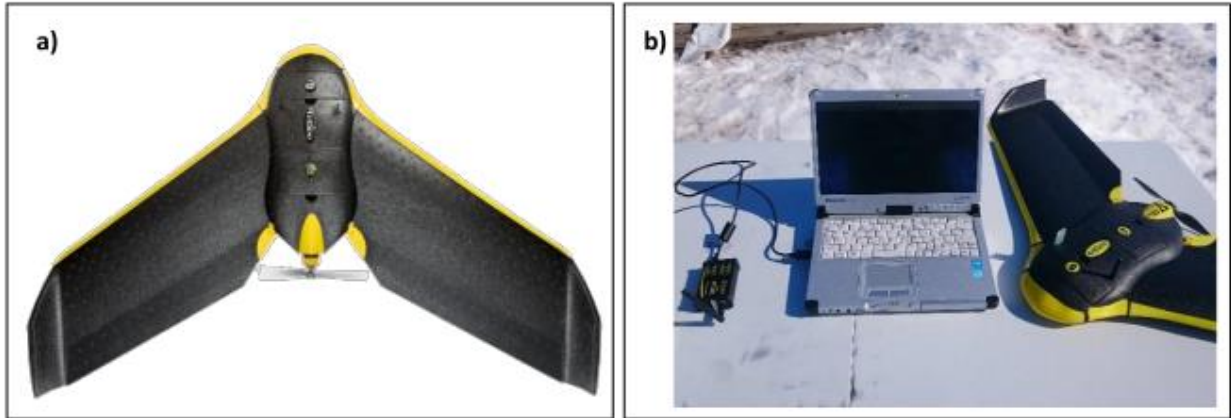
Sensefly EBEE AG specifications	
Maximum flight time	45 minutes
Nominal cruise speed	40-90 km/h (11-25 m/s)
Radio link range	Up to 3 km
Wind resistance	Up to 45 km/h (12m/s)
Ground Sampling Distance (GSD)	Down to 2 cm per pixel
Relative orthomosaic/3D model accuracy	1-3 x GSD
Absolute horizontal/vertical accuracy (w/GCPs)	Down to 4 cm / 7 cm
Absolute horizontal/vertical accuracy (no GCPs)	1-5 m
UAV flight parameters	
Areal extent of flight	2.2 km^2 / 222 ha
Number of flights	2
Elevation (A.T.O)	100 m
Ground Sampling Distance (GSD)	3.3 - 3.6 cm
Ground Control Points added	12
GCP accuracy	0.002 m
Estimated horizontal/ vertical accuracy (after GCPs)	2-10 cm
Number of photos per flight	656 - 757
Image overlap (Vertical / horizontal %)	70 / 80
Camera payload	
Sony DSC-WX220_4.4_4896x3672 (RGB)	Sensor Dimensions (mm): 6.170 x 4.627
Canon CanonPowerShotELPH110HS_4.3_4608x3456 (RGB)	Sensor Dimensions (mm): 6.172 x 4.629

Appendix 3: Ground control point (left) marker for correcting UAS georeferencing in SfM software Postflight Terra 3D (now Pix4D). B. Walker tagging GCP using Leica GNSS RTK rover (right). GCPs were resurveyed for each UAS flight.

Appendix 4: Summary of UAS flights, magnaprobe snow depth surveys and snow core depth and density measurements collected across the 2016 spring melt period. UAS snow depth and SWE were estimated using observations collected on the same date as the UAS flight. For instances where no snow observations were collected on the same date as a UAS flight the nearest observations were used.

Date	UAS snow depth	Magnaprobe snow depths (n)	Depth and density sites (n)
23-Apr-16	■	1339	20
24-Apr-16			
25-Apr-16			
26-Apr-16			
27-Apr-16	■		
28-Apr-16	■	377	20
29-Apr-16	■	379	
30-Apr-16	■	753	
01-May-16		385	10
02-May-16			
03-May-16			
04-May-16	■	676	
05-May-16	■	434	
06-May-16			11
07-May-16			
08-May-16	■		
09-May-16		538	11
10-May-16	■		
11-May-16		477	7
12-May-16	■	475	
13-May-16	■		4
14-May-16			
15-May-16			
16-May-16			
17-May-16		132	1
18-May-16	■		
19-May-16	■		
20-May-16			
21-May-16	■		

■	Successful UAS snow depth map produced
n	Magnaprobe snow depths collected
n	Snow core depth and density survey collected